CHAPTER 3

RESULTS

The results obtained from geophysical measurement in this thesis research will be explained in the following sequences; Ground penetrating radar, magnetic mapping, resistivity mapping, and CVES.

3.1. Ground penetrating radar

3.1.1 Velocity analysis

In order to convert time section of a radargram to depth section of the radar section, velocity of radar signal in the ground should be known. Since the reflections of a small object in the ground normally appear as hyperbolic-shape reflection in radar sections, the RMS velocity of radar signal in the ground will be determined from hyperbola fitting as shown in Figure 3.1.

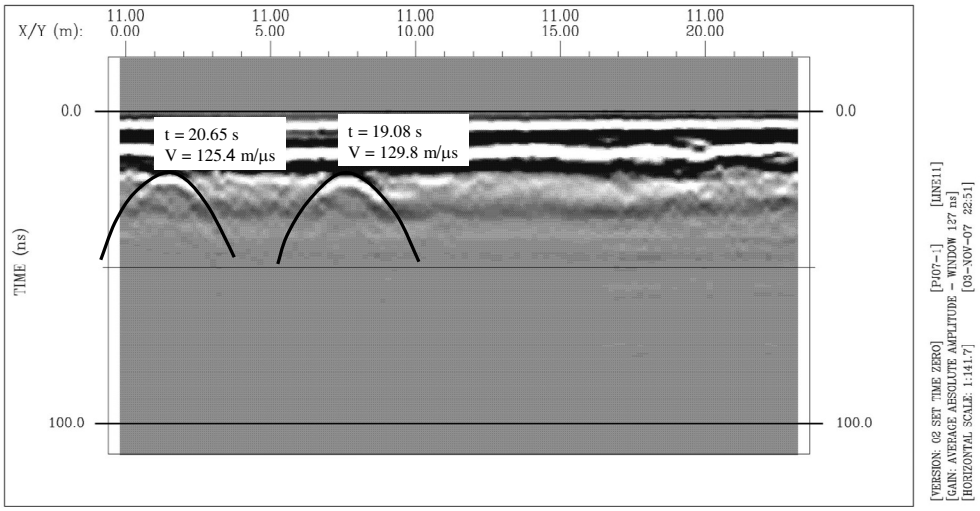

Figure 3.1 Hyperbola fitting for LineA-11

3.1.1.1 Sub-area A

Hyperbola fitting was conducted on 18 hyperbolas in profiles of this sub-area. The resulted velocity ranges from 94.22 to 153.14 m/μs with a mean velocity of 125.37 ±17.14 m/μs. Distribution of the velocities is also shown in Figure 3.2 (a). Therefore, a velocity of 125 m/μs was applied for converting time section to depth section in all radar profiles.

3.1.1.2 Sub-area B

The total numbers of 14 hyperbolas were used for hyperbolic fitting in this sub-area. The resulted velocity ranges from 93.97 to 147.10 m/μs with a mean velocity of 120.65 ±14.24 m/μs. Distribution of the velocity is also shown in Figure 3.2 (b). A velocity of 121 m/μs was then applied for converting time section to depth section.

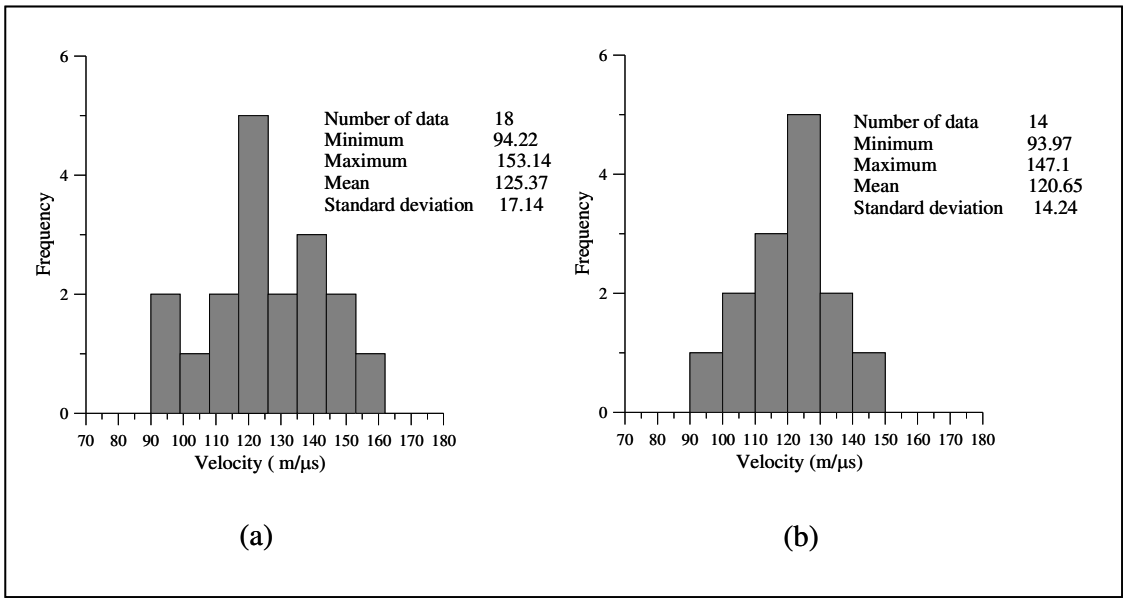

Figure 3.2 Velocity distributions (a) in sub-area A and (b) in sub-area B

3.2.2 GPR Interpretation.

In displayed radar sections, X and Y on the horizontal axis denote line number and distance along measurement lines respectively, whereas depth from the surface is shown on the vertical axis. Dash lines in radar sections denote interpreted boundaries between soil layers and hyperbolic shape curves denote reflection anomalies. Three layers of soils can be distinguished clearly from reflection pattern of radargrams. They are top, middle, and bottom layers.

In the top layer, no reflected anomaly was observed. This probably indicates homogeneity of the soil. The thickness of this layer varies from 0.4 to 0.9 m. In average, its thickness is approximately 0.5 m. This layer was interpreted as topsoil.

In the middle layer which underlies the topsoil, many hyperbolic-shape reflections and discontinuity of radar signals were observed. These indicate that there are many disturbances in this layer which might be related to human activities in the past. Archaeological excavation conducted in this area of study found that most of artifacts were buried at this layer. The thickness of this layer varies between 0.6 and 1.5 m. This layer corresponds with the cultural layer in Källén's work and it will be focused in the present study.

In this middle layer, disturbed zones are interpreted as disturbed soil which associated with human activities in the past. Artifacts were expected to be buried in these zones. In addition, hyperbolic shape reflections observed in this layer are interpreted as artifacts such as ceramic vessels; fired clay, big conglomerate, and bulks of stone. Typical soil profiles obtained from archaeological excavation in vicinity of this study area by Källén (2004) are shown in Figure 1.23.

In the bottom layer which underlies the cultural layer, small number of reflection anomalies was observed; this probably indicates homogeneity of the soil in this layer. This layer may correspond with sterile soil in Källén's work. The depth to this layer ranges between 1.5 and 2.2 m. However, at the boundary between the cultural layer and this sterile soil, some reflection anomalies were observed. These are

probably caused by small bulks of slate, packs of laterite. The radar results agreed with archaeological excavation conducted by Källén during 2003 and 2004.

3.2.2.1 Sub-area A

Radar sections and their interpretations of all lines of measurement in sub-area A are shown in Figures 3.3 to 3.13. Locations of radar discontinuity zones and hyperbolic anomalies observed in the middle layer or "cultural layer" are summarized in Table 3.1 and Table 3.2 respectively.

Table 3.1 Locations of discontinuity zones in the middle layer of sub-areas A

Line no.	Discontinuous zones	Distance (m)	Depth (m)
A-05	D1	10.5 to 15.8	1.6
A-06	D1	11.0 to 17.0	1.6
A-07	D1	10.5 to 17.0	1.8
A-08	D1	12.5 to 16.5	1.8
A-10	D2	8.2 to 9.8	1.2
A-11	D2	8.2 to 9.8	1.3
A-18	D3	1.6 to 5.8	1.2
A-19	D3	4.6 to 6.0	1.2
A-20	D3	2.0 to 6.0	1.2
A-21	D3	3 to 6.0	1.2
A-22	D3	3 to 7.8	1.2
A-22	D4	17.8 to 22.8	1.5
A-23	D4	17.0 to 21.0	1.5
A-24	D5	4.0 to 7.0	1.3
A-25	D6	13.8 to 16.8	1.3
A-26	D6	12.8 to 16.0	1.3
A-27	D6	13.2 to 16.8	1.3

Table 3.2 Locations of hyperbolic anomalies in the middle layer of sub-areas A

Line no.	Hyperbolic shapes (distance in meter, depth in meters)
A-00	H1(0.5,0.6)
A-01	H2(1.8,1.0); H3(9.7,1.3)
A-02	H4(6.8,1.0); H5(7.6,1.0); H6(9.0,1.0);H7(16.1,0.8)
A-03	H8(4.0,1.1); H9(11.4,1.4); H10(16.5,0.6)
A-04	H11(3.1,1.0)
A-05	H12(21.5,0.8)
A-08	H13(1.2,1.1); H14(4.0,1.1); H15(18.5,0.9)
A-09	H16(19.0,0.8)
A-10	H17(19.2,0.9)
A-11	H18(1.6,1.3); H19(7.6,1.3)
A-12	H20(11.0,1.2); H21(16.6,0.9); H22(21.8,0.9)
A-14	H23(6.0,1.1); H24(21.0,1.9)
A-15	H25(6.5,1.0)
A-16	H26(17.4,0.9); H27(22.0,0.9)
A-17	H28(6.5,1.0)
A-18	H29(17.4,0.8)
A-22	H30(19.5,1.5)
A-28	H31(1.6,1.2); H32(8.2,0.6); H33(12.6,0.7)
A-29,	H34(12.0,0.5)

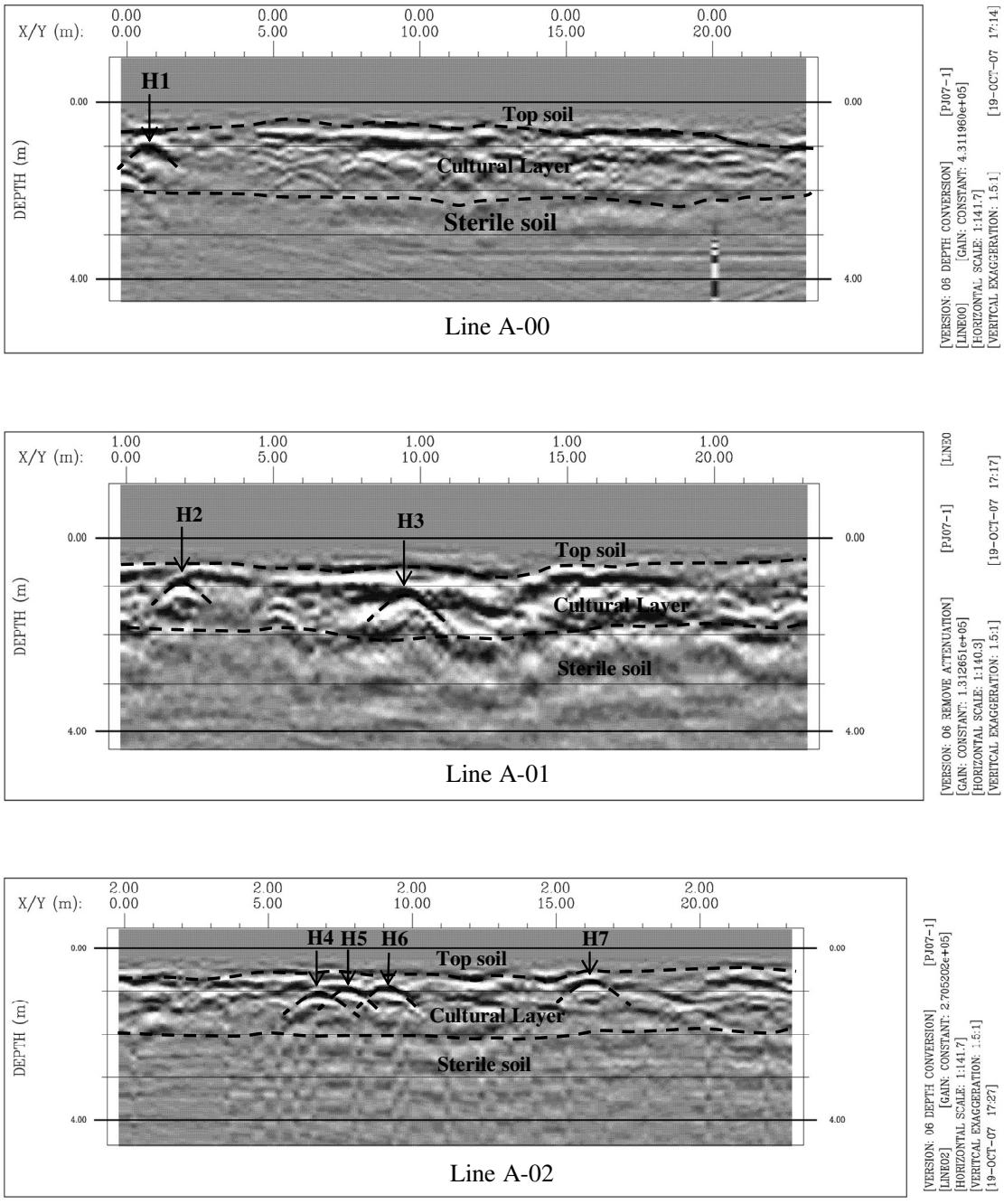

Figure 3.3 Radar section of Line A-00 to A-02

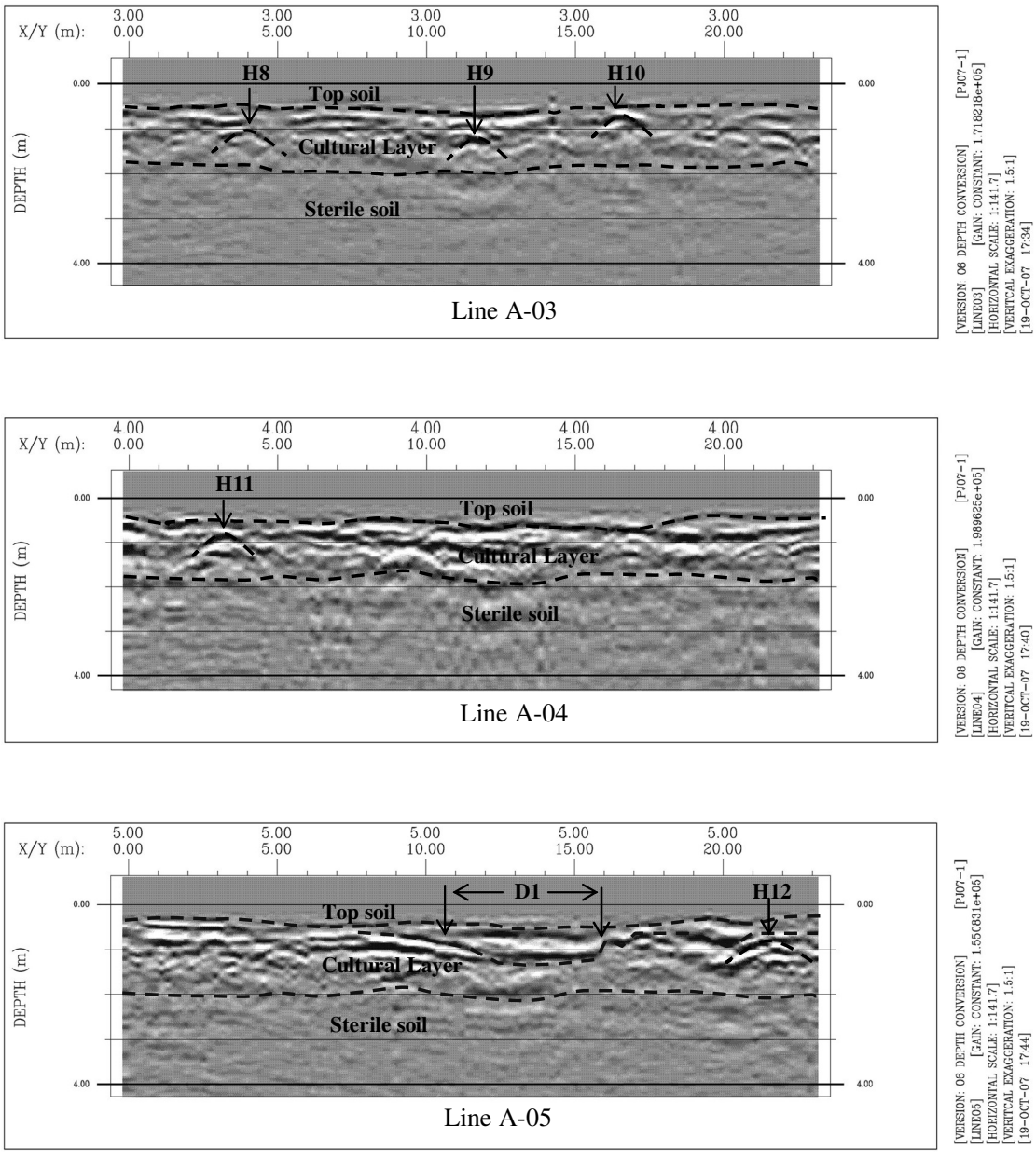

Figure3.4 Radar section of Line A-03 to A-05

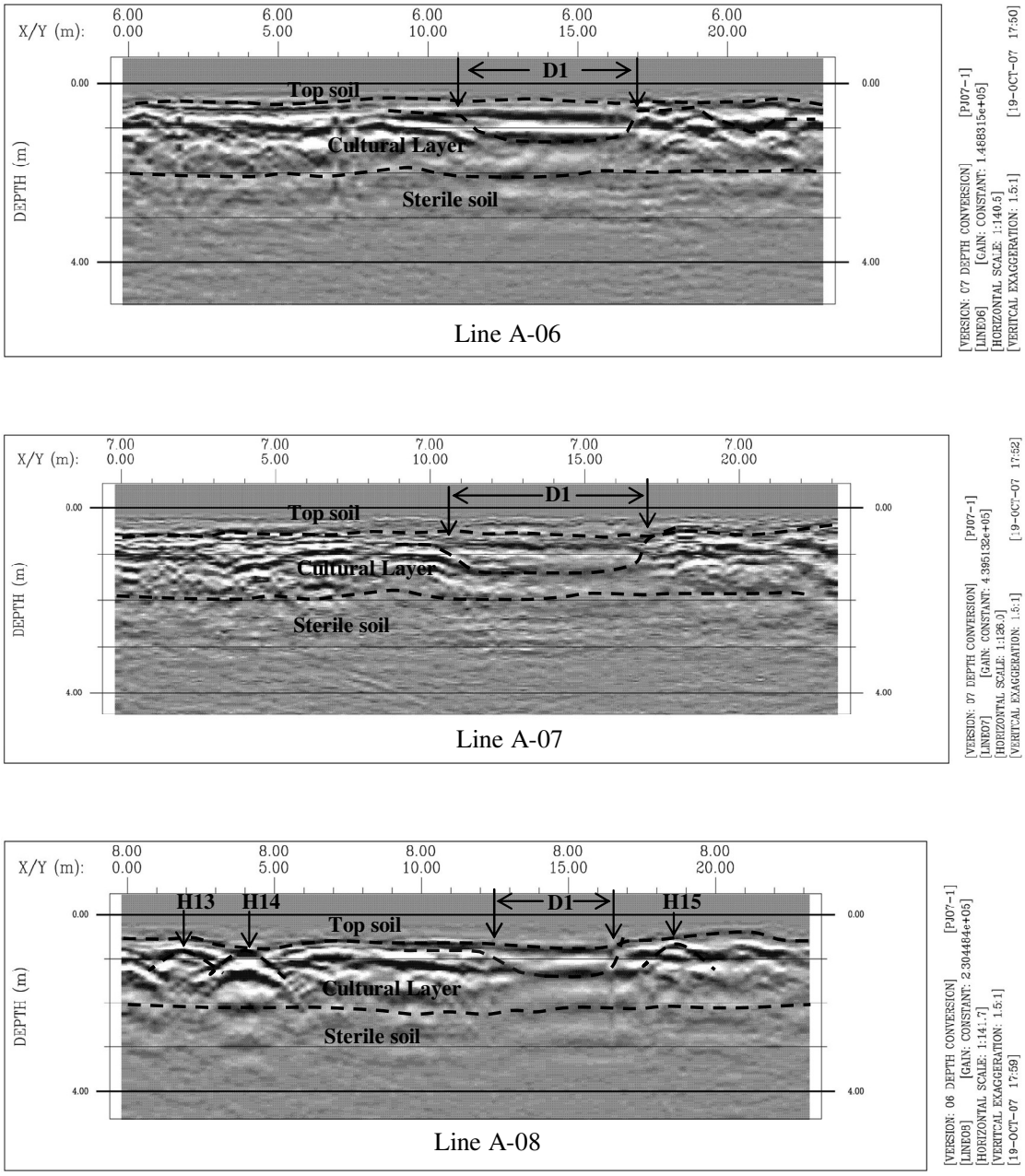

Figure3.16 Radar section of Line A-06 to A-08

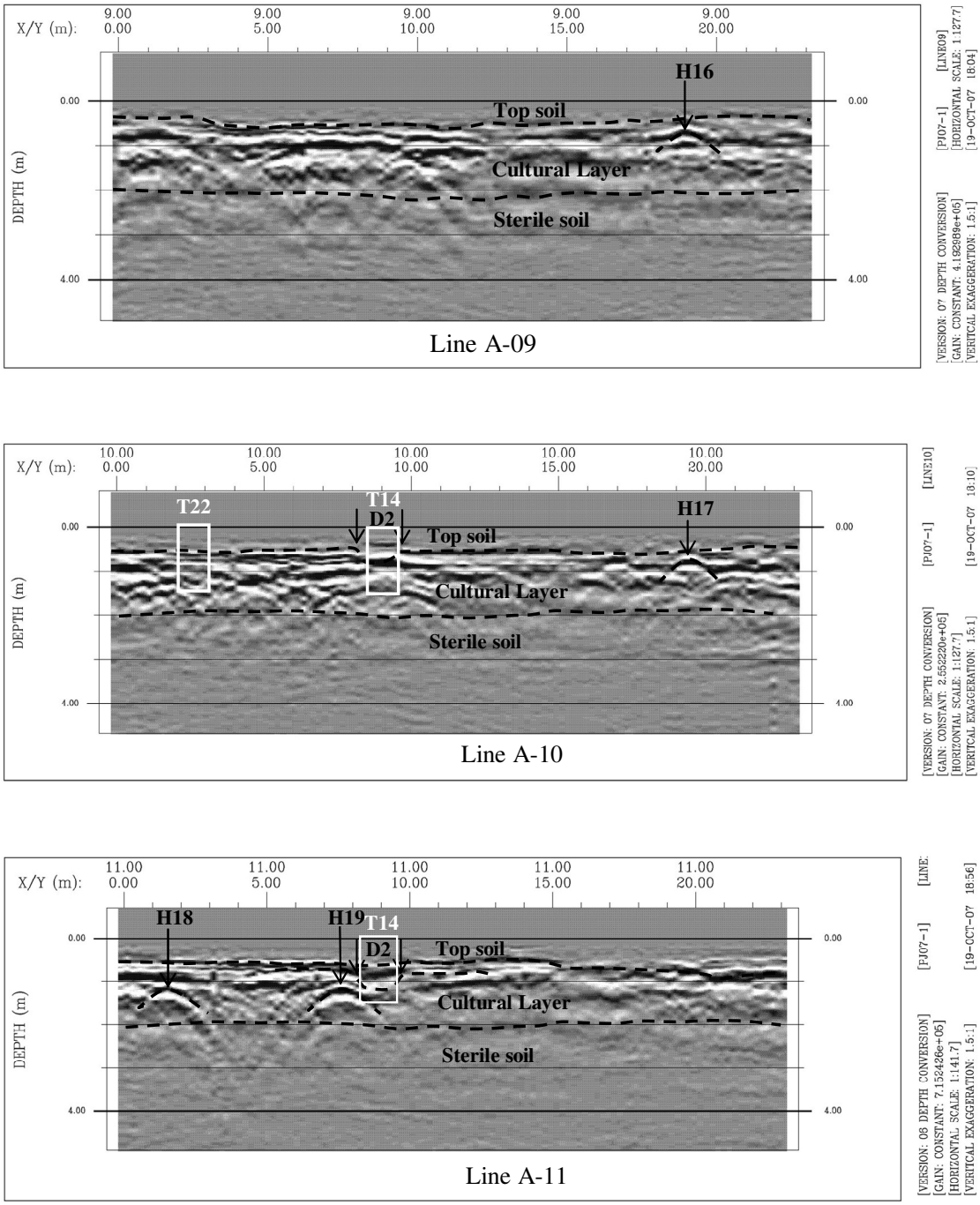

Figure3.17 Radar section of Line A-09 to A-11

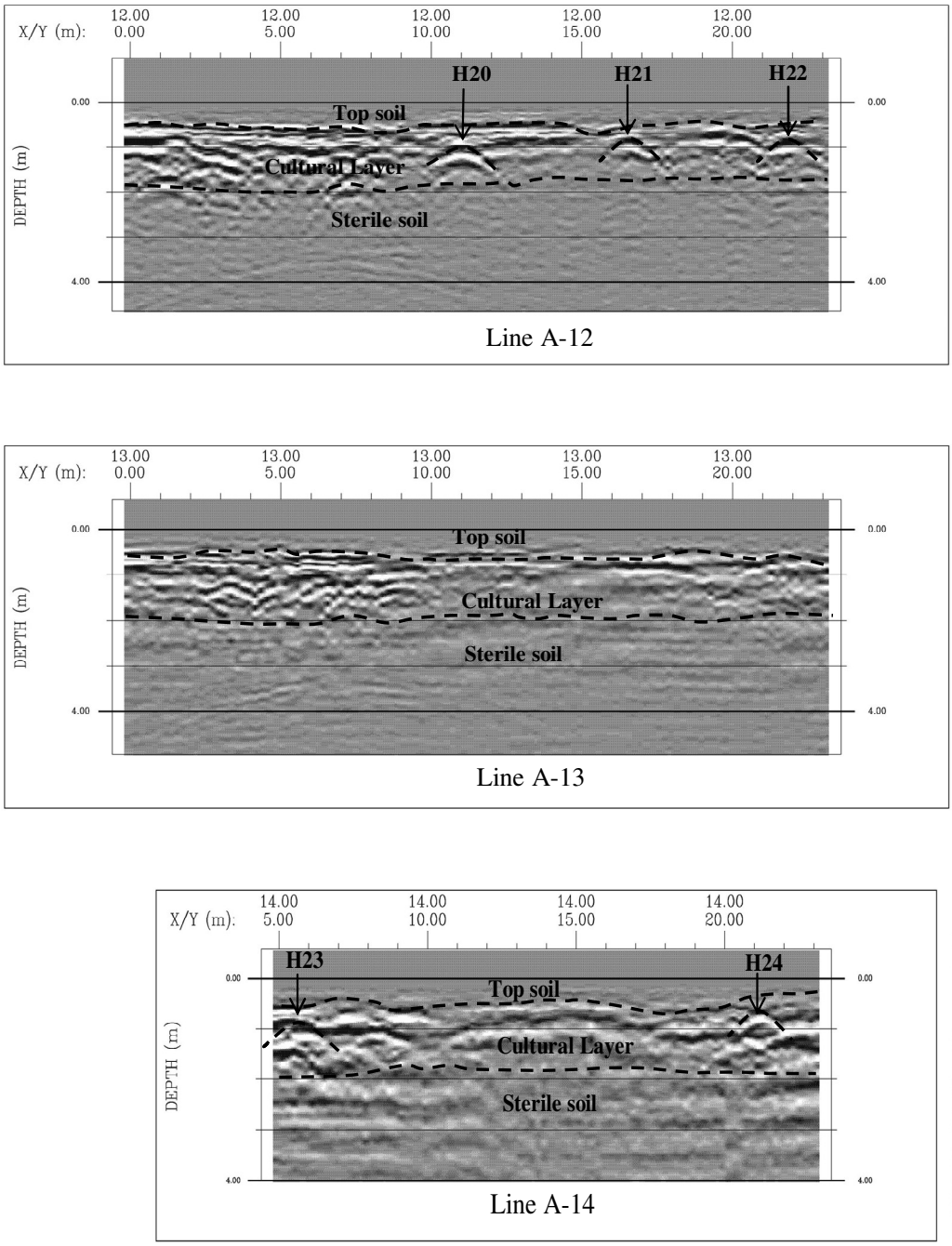

Figure 3.7 Radar section of Line A-12 to 14

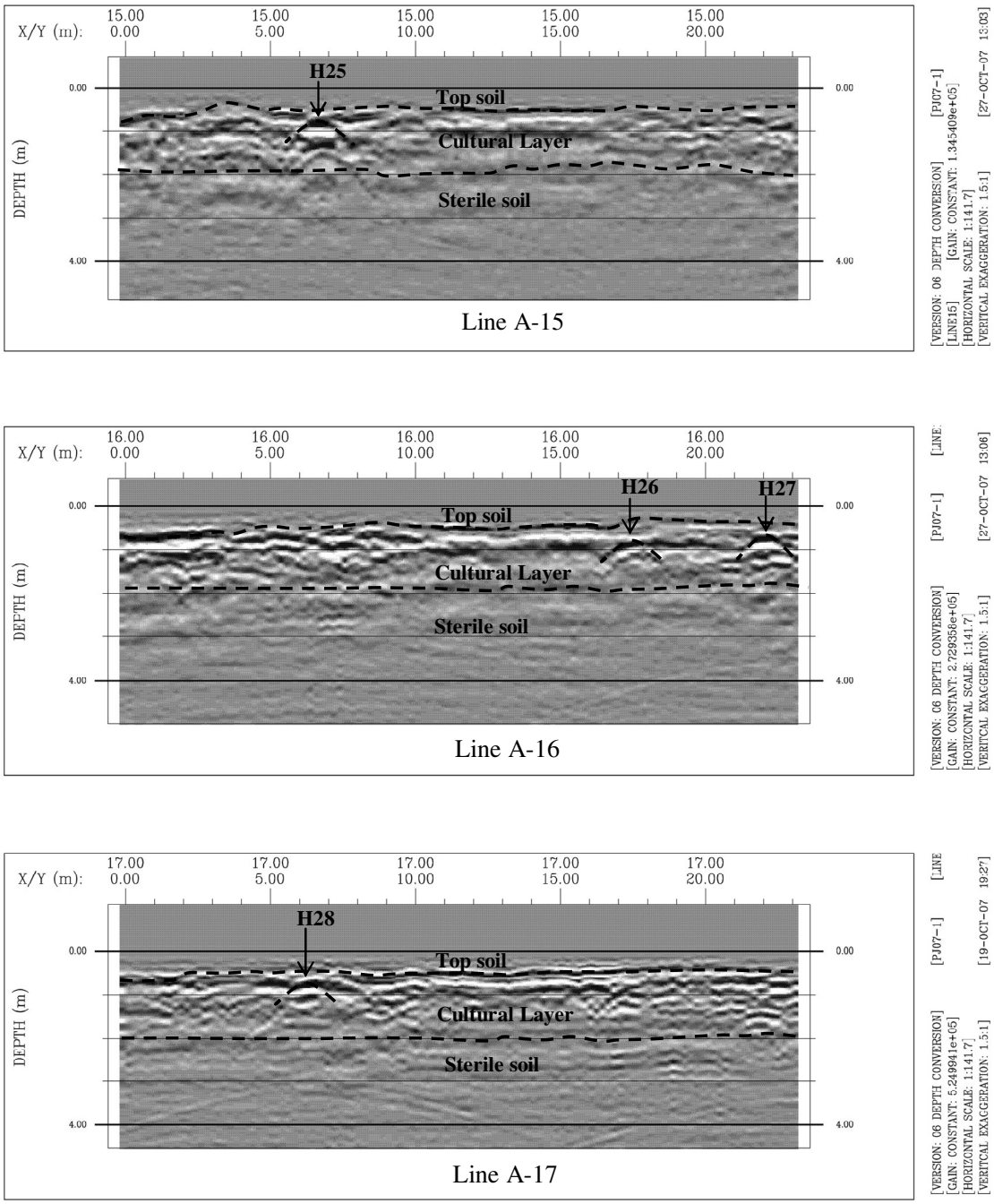

Figure 3.8 Radar section of Line A-15 to A-17

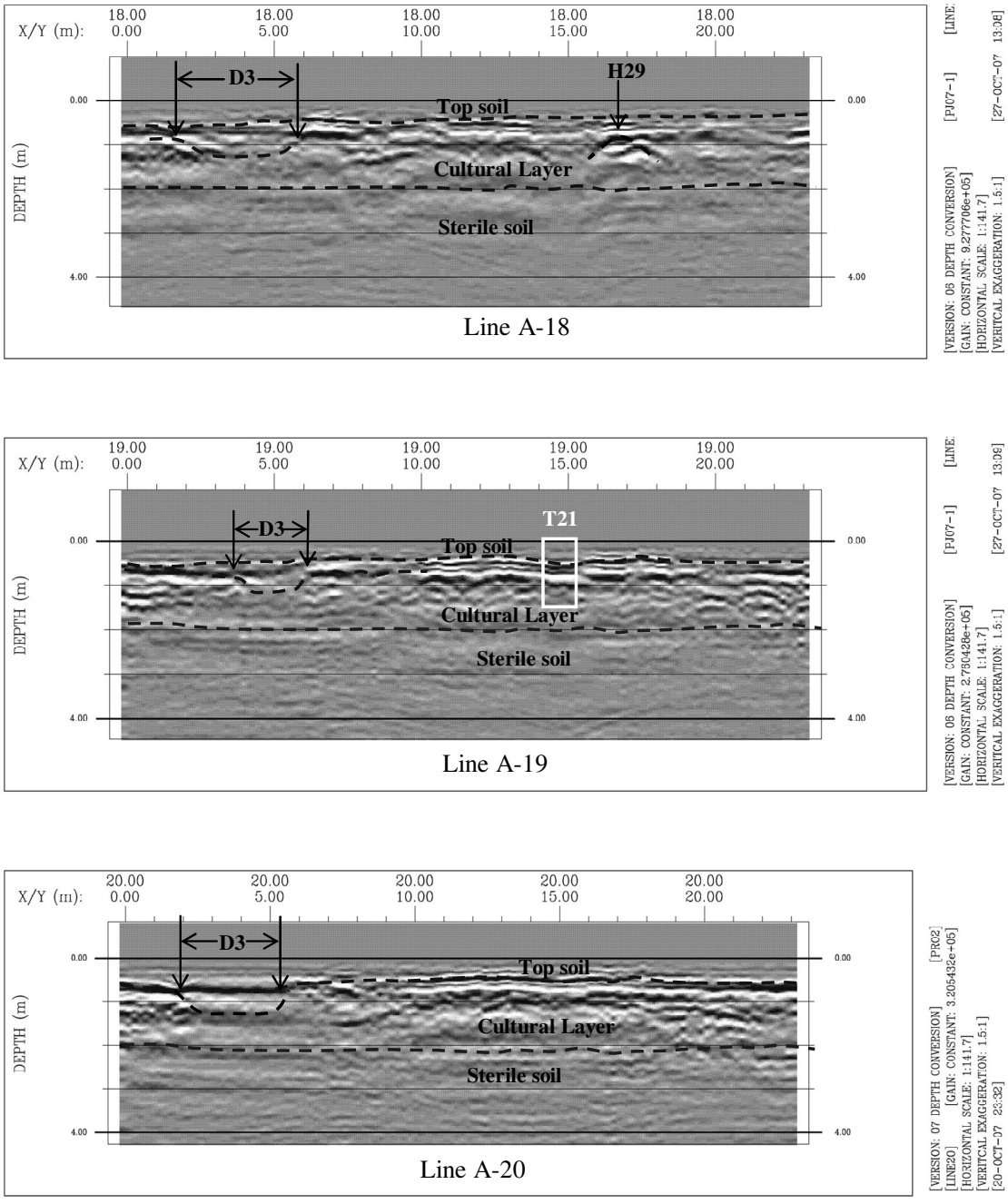

Figure 3.9 Radar section of Line A-18 to A-20

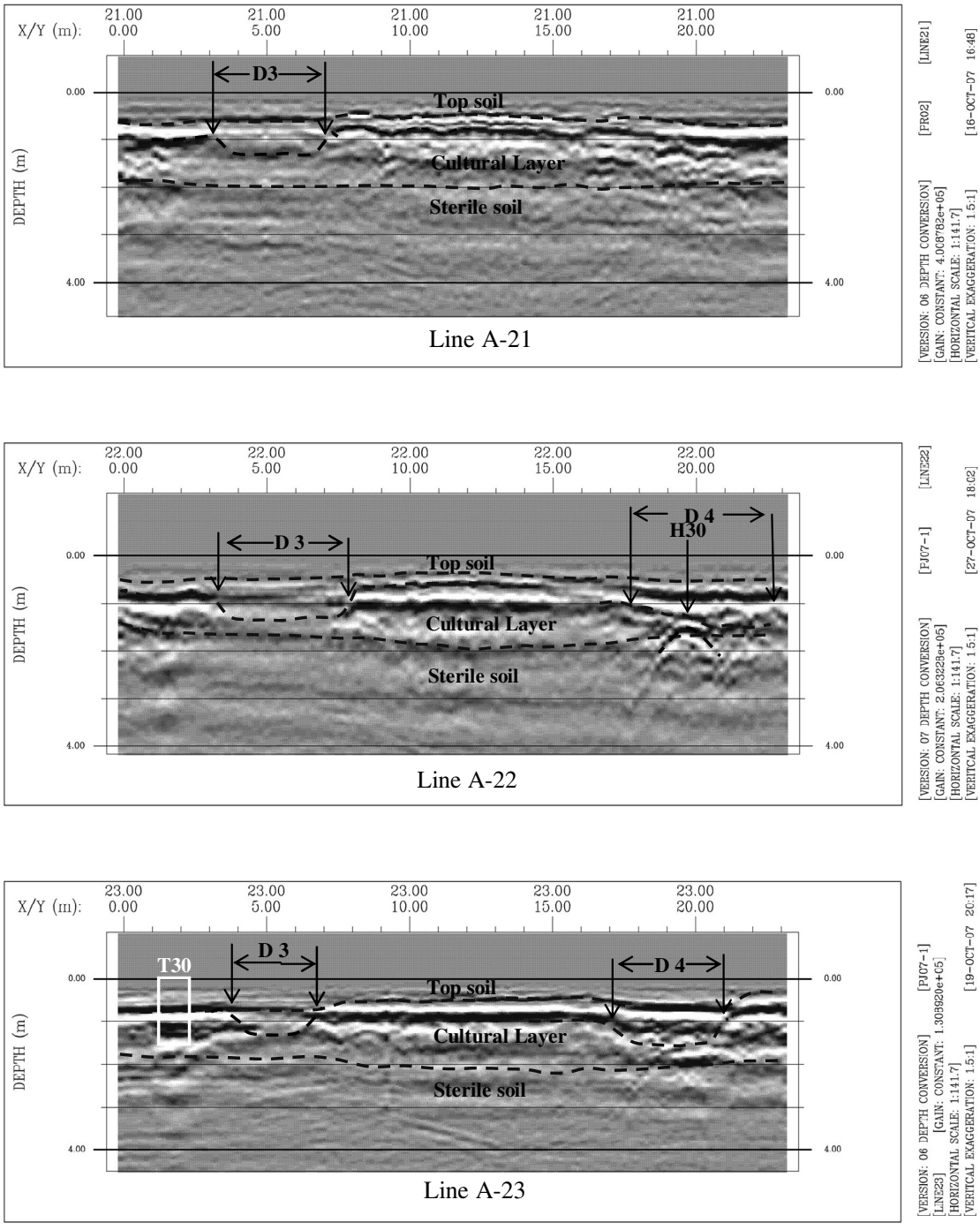

Figure 3.10 Radar section of Line A-23 to A-23

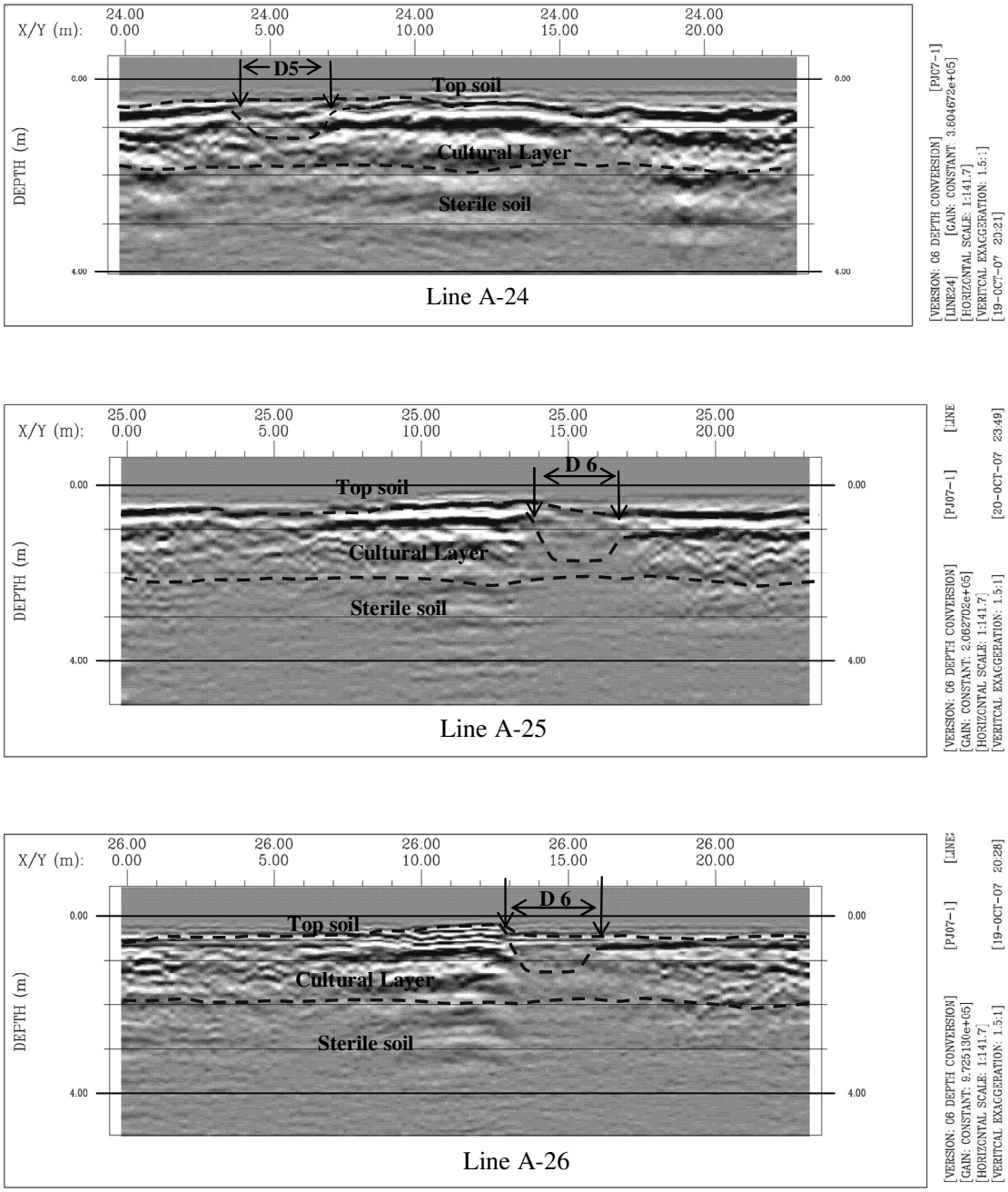

Figure 3.11 Radar section of Line A-24 to A-26

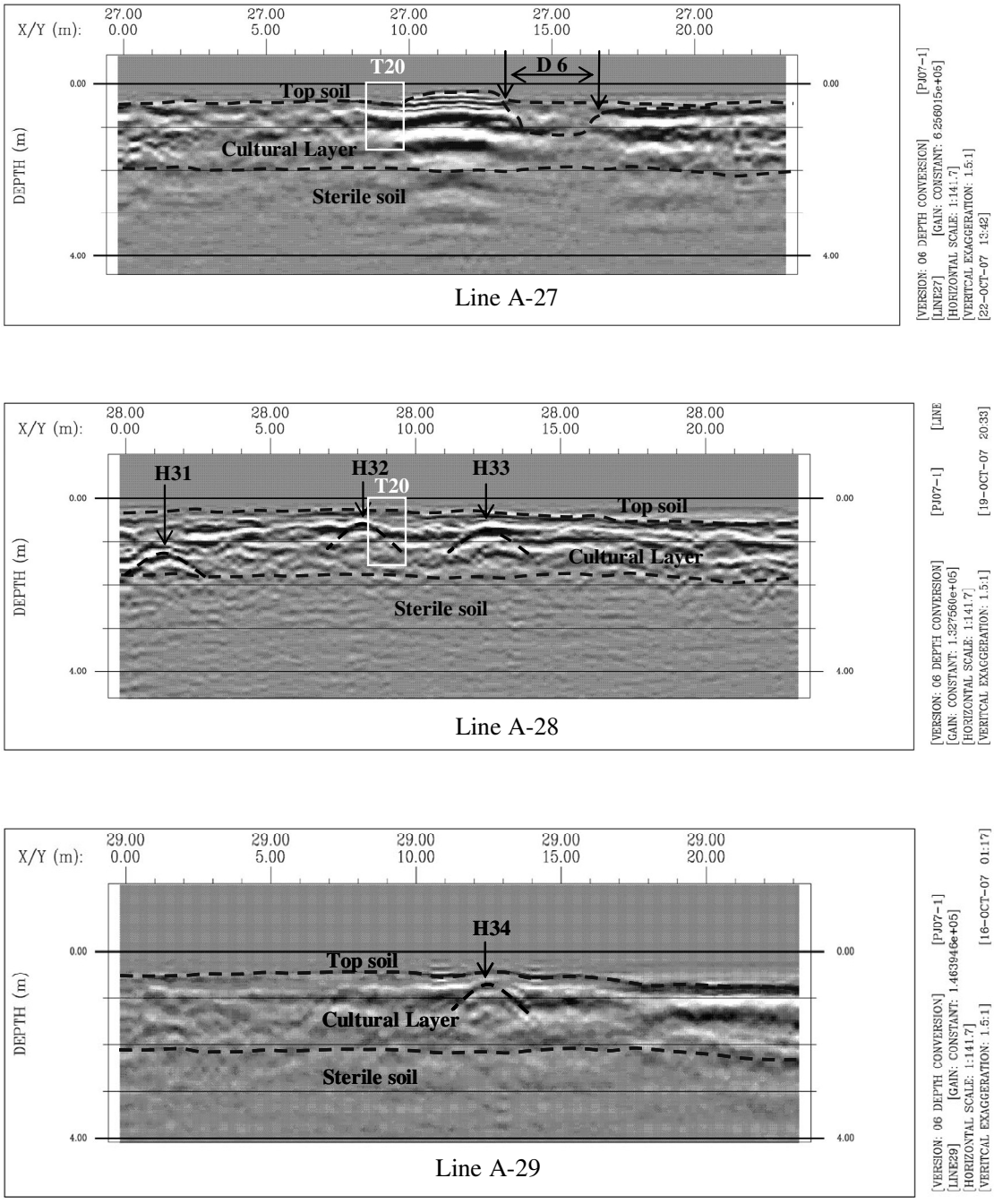

Figure 3.12 Radar section of Line A-27 to A-29

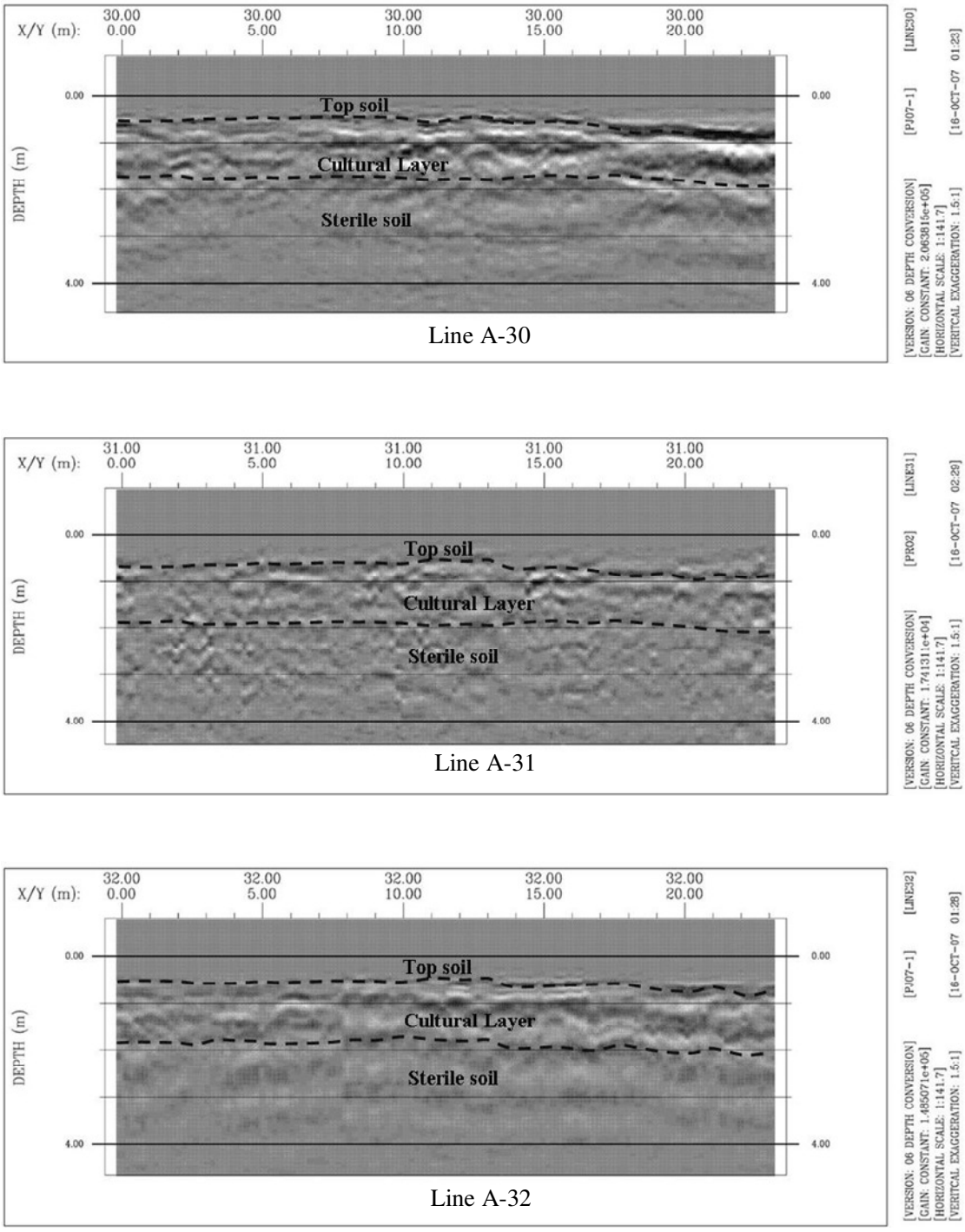

Figure 3.13 Radar section of Line A-30 to A-32

3.2.2.2 Sub-area B

Radar sections and their interpretations of all lines of measurement in sub-area B are shown in Figures 3.14 to 3.23. Locations of radar discontinuity zones and hyperbolic anomalies observed in the middle layer or "cultural layer" are summarized in Table 3.3 and Table 3.4 respectively.

Table 3.3 Locations of discontinuity zones in the middle layer of sub-areas B

Line no.	Discontinuous zones	Distance (m)	Depth (m)
B-03	D7	6.0 to 8.8	1.3
B-04	D7	5.4 to 7.6	1.4
B-03	D8	13.1 to 15.8	1.2
B-04	D8	14.2 to 18.4	1.2
B-05	D8	15.4 to 19.8	1.3
B-06	D8	16.0 to 22.0	1.5
B-07	D8	16.8 to 20.2	1.5
B-08	D8	17.0 to 20.0	1.5
B-09	D8	17.1 to 22.0	1.5
B-10	D8	17.2 to 20.0	1.5
B-11	D8	16.7 to 22.0	1.2
B-12	D8	15.9 to 22.0	1.5
B-13	D8	15.2 to 20.0	1.3
B-08	D9	9.5 to 11.0	1.2
B-10	D10	9.0 to 11.2	1.5
B-10	D11	1.4 to 5.0	1.4
B-10	D12	7.5 to 10.0	1.6
B-14	D13	1.8 to 10.2	1.5
B-14	D14	13.8 to 17.0	1.4

Locations of the hyperbolic anomalies are (labeled H36 to H46) are summarized in Table 3.4.

Table 3.4 Locations of hyperbolic anomalies in the middle layer of sub-areas B

Line no.	Hyperbolic shapes (distance in meter, depth in meters)
B-00	H35(8.0, 0.8)
B-02	H36(7.8,1.1); H37(21.0,1.8)
B-15	H38 (1.4,1.6); H39(4.5,1.5); H40(10.0,1.0)
B-16	H41(12.5, 1.1)
B-17	H42(6.0, 1.1)
B-25	H43(15.0, 1.9) H44(16.2, 1.2)
B-26	H45(8.2, 0.9); H46(12.5, 1.0); H47(14.5, 1.0)

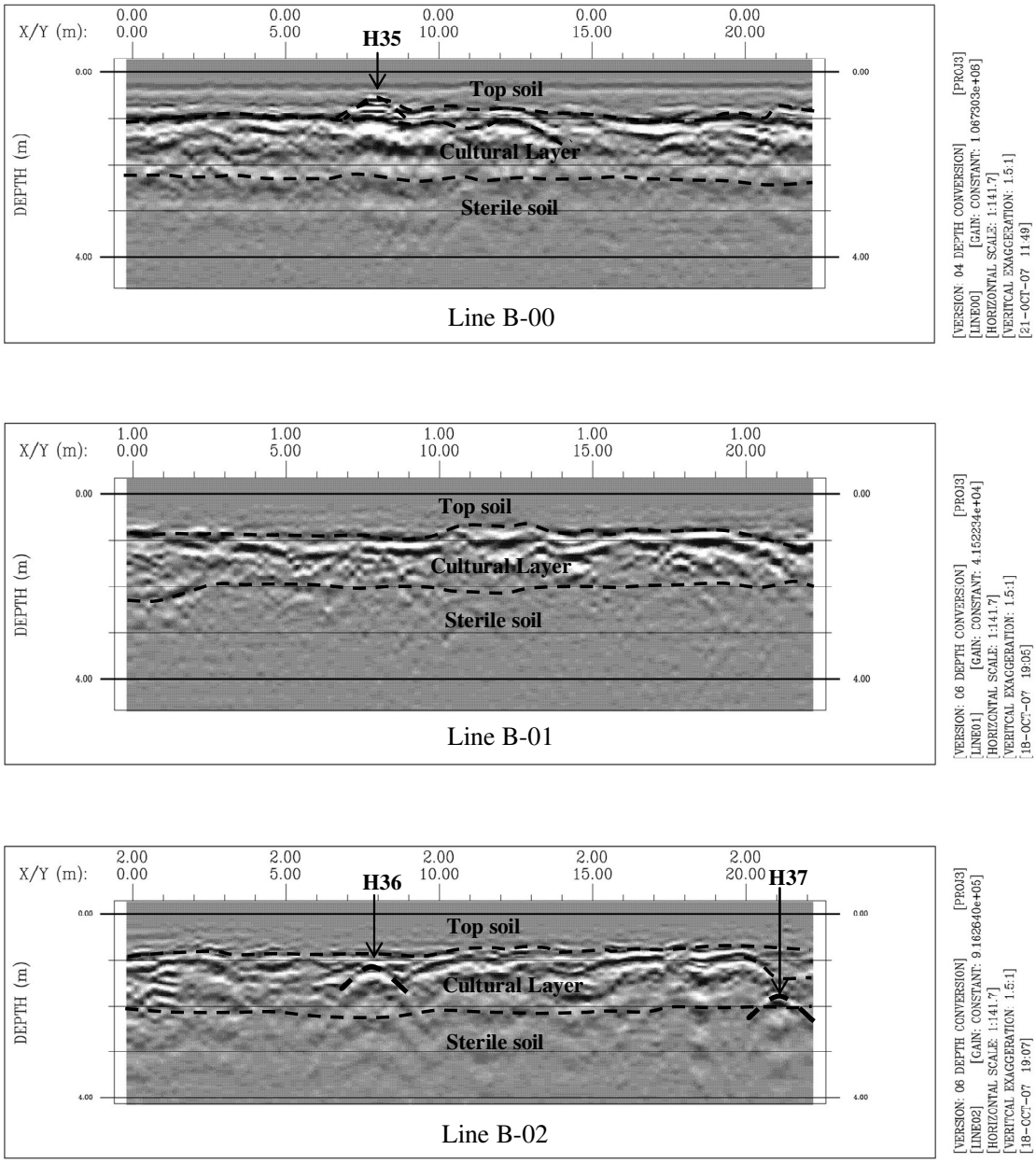

Figure 3.14 Radar section of Line B-00 to B-02

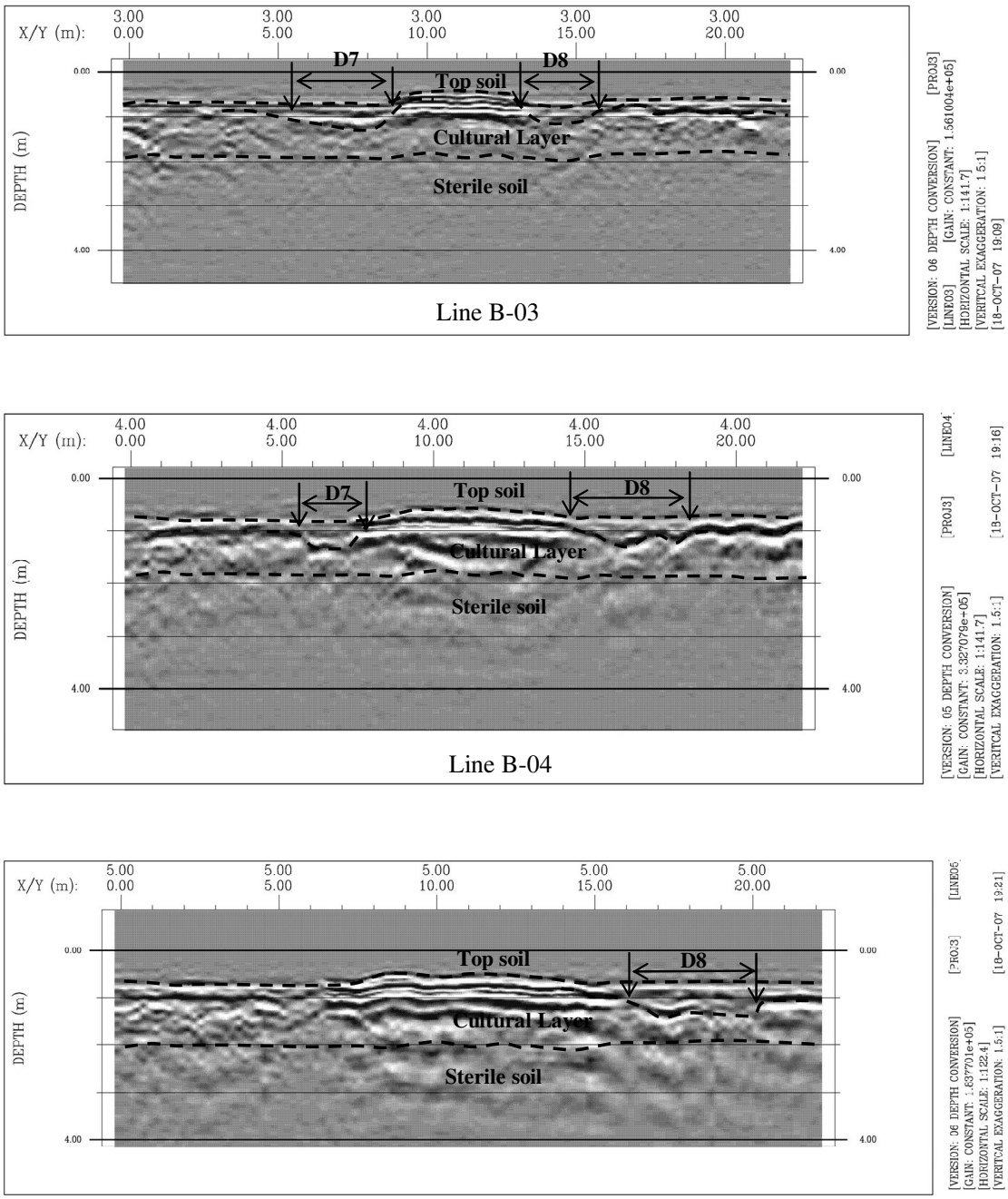

Figure 3.15 Radar section of Line B-03 to B-05

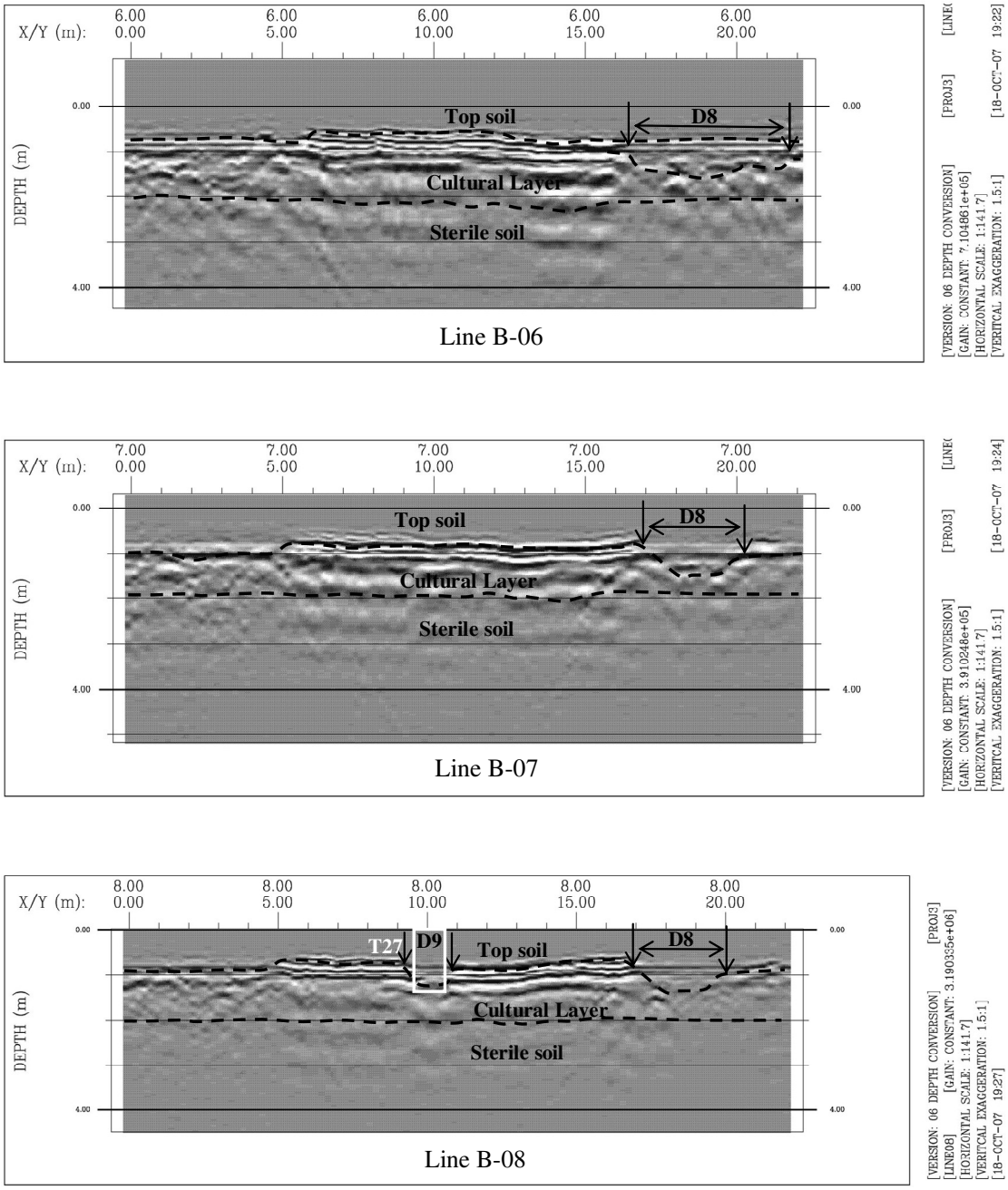

Figure3.16 Radar section of Line B-06 to B-08

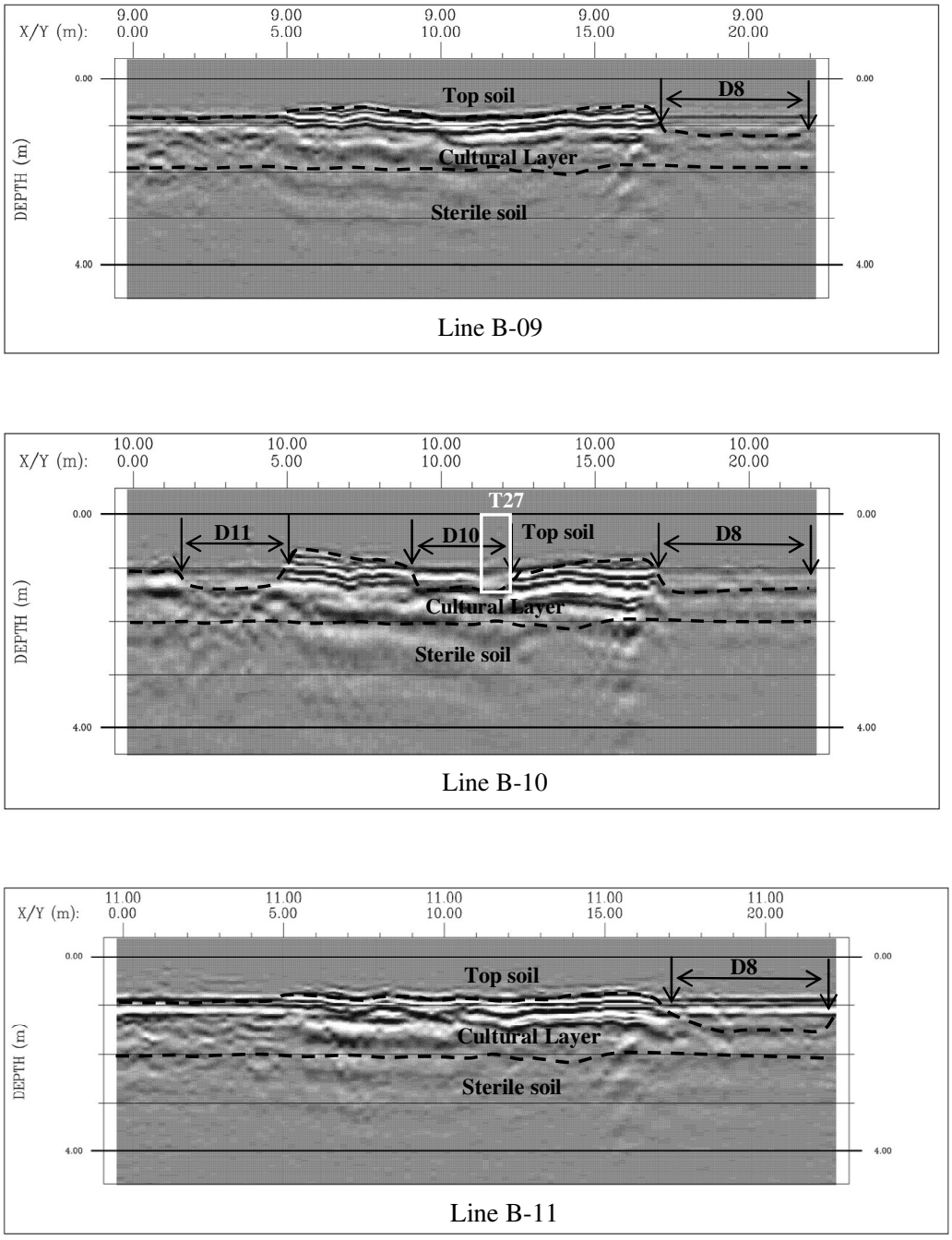

Figure3.17 Radar section of Line B-09 to B-11

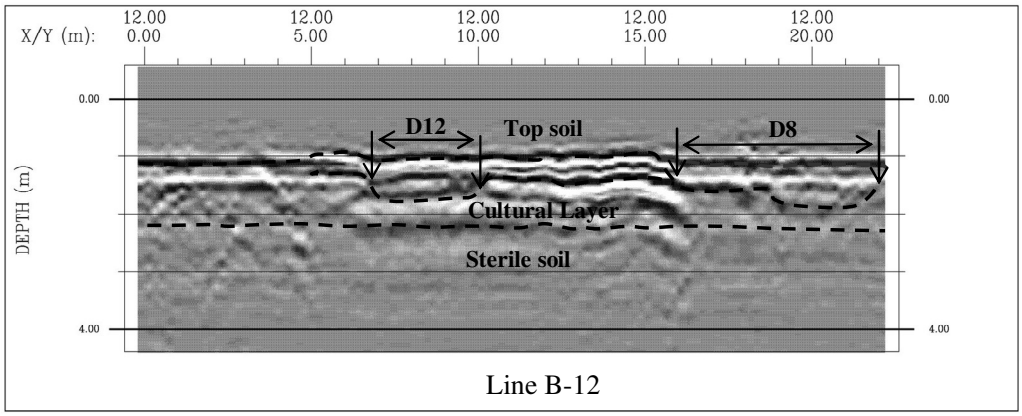

Line B-12

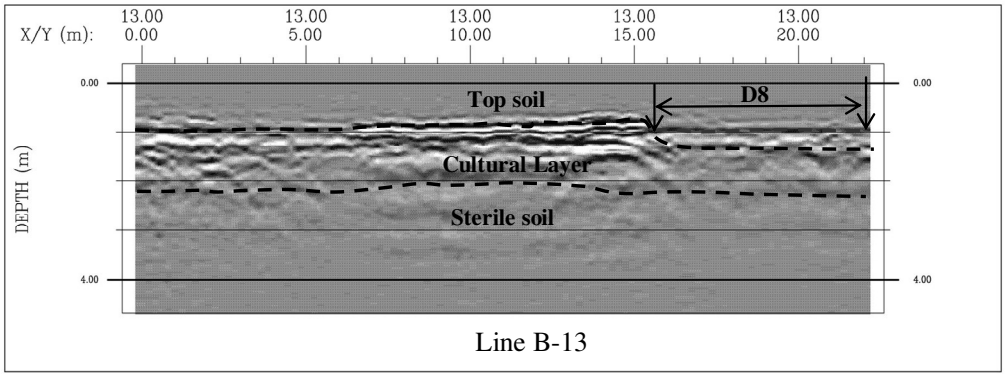

Line B-13

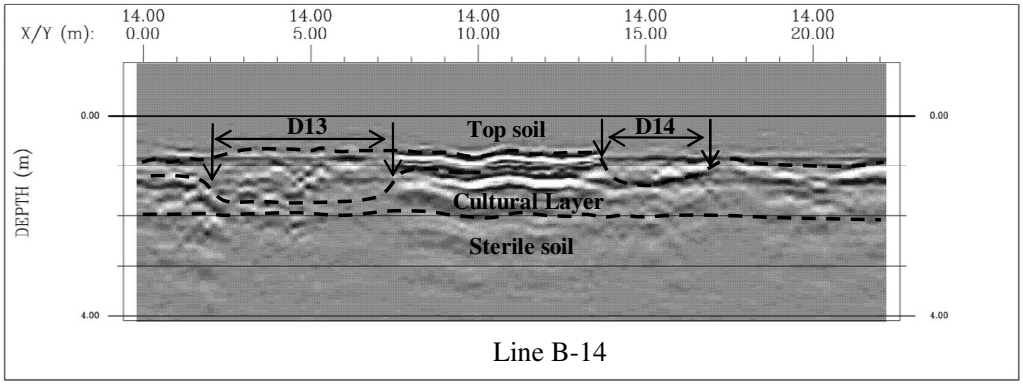

Line B-14

Figure 3.18 Radar section of Line B-12 to B-14

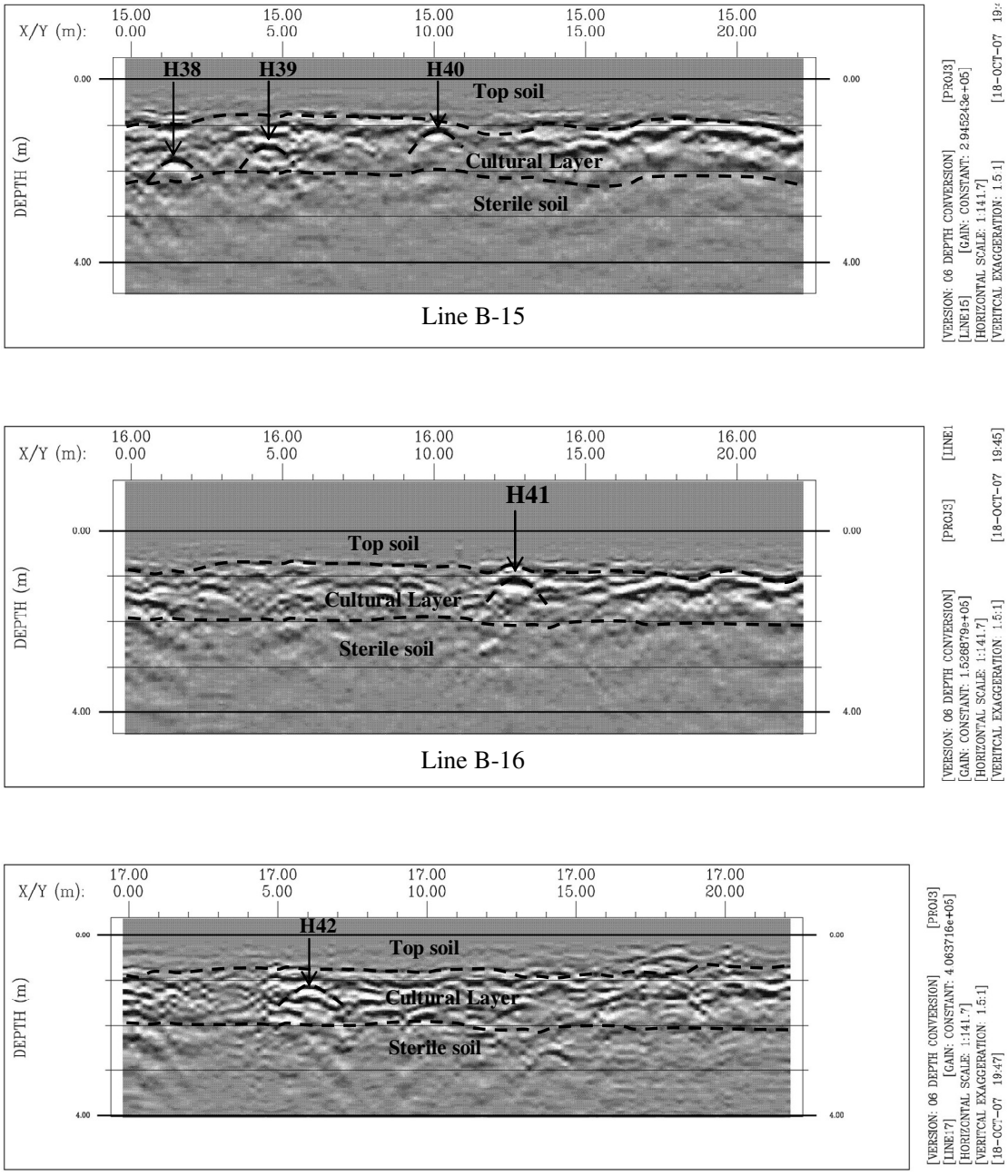

Figure 3.19 Radar section of Line B-15 to B-17

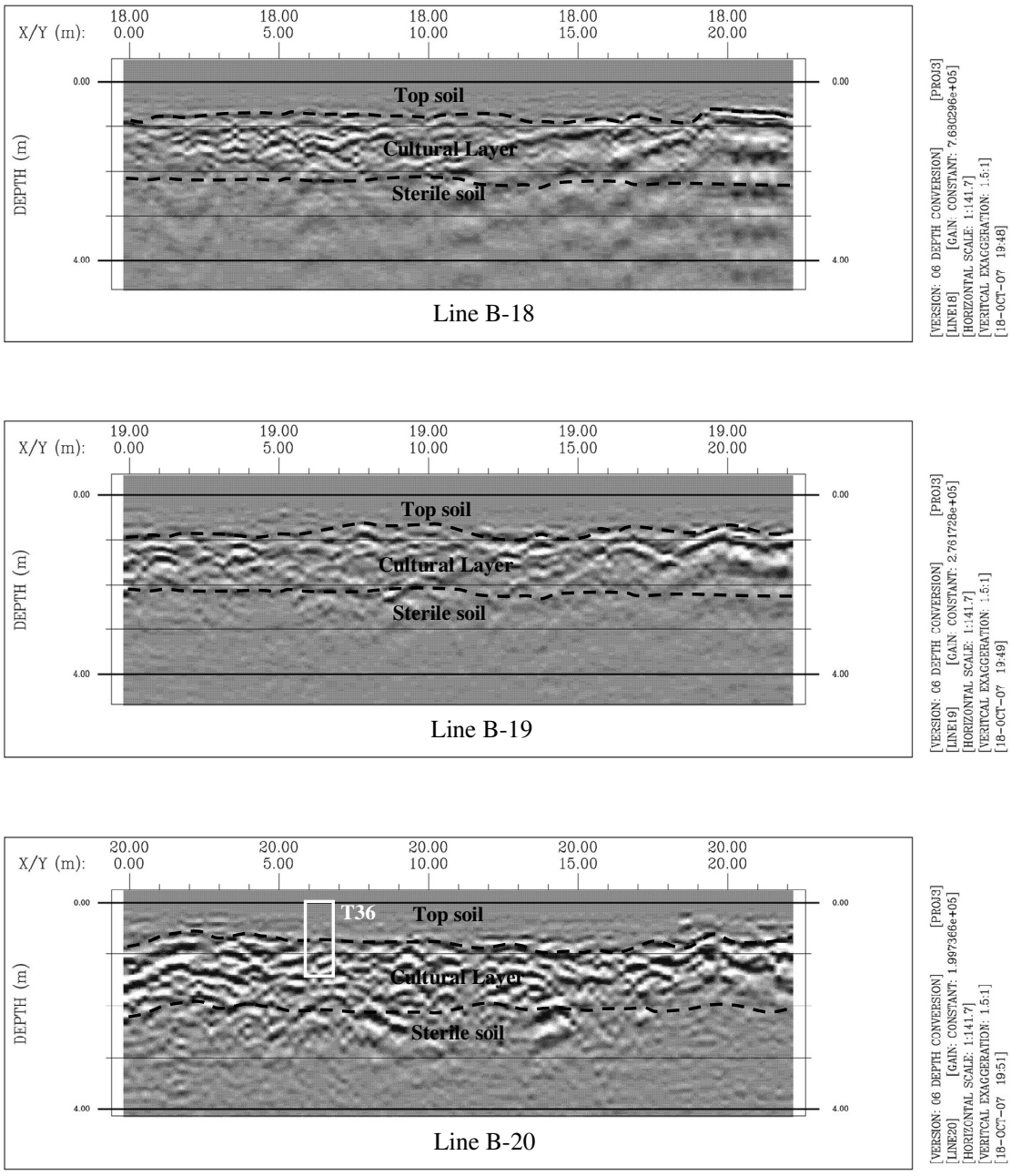

Figure 3.20 Radar section of Line B-18 to B-20

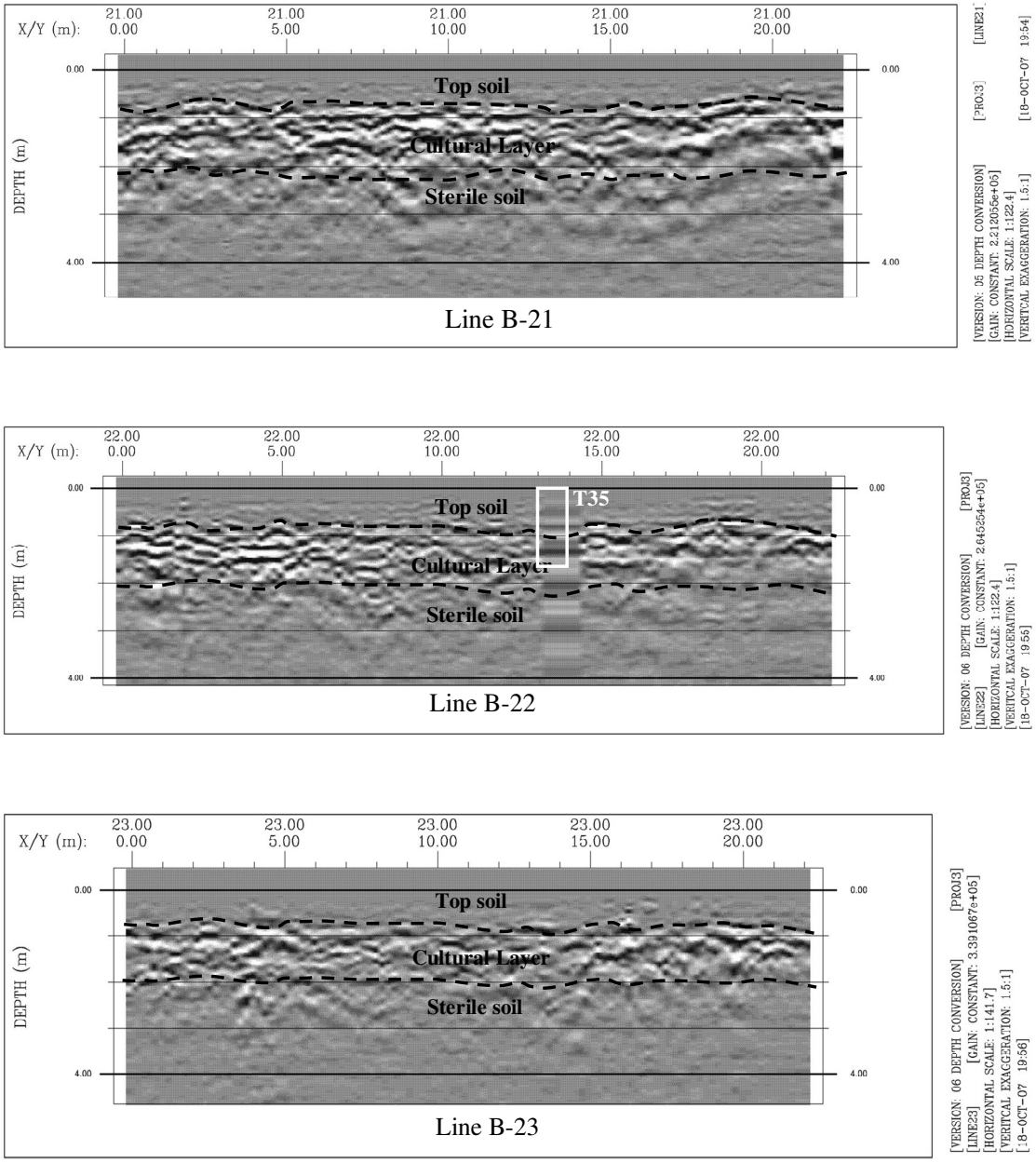

Figure 3.21 Radar section of Line B-21 to B-23

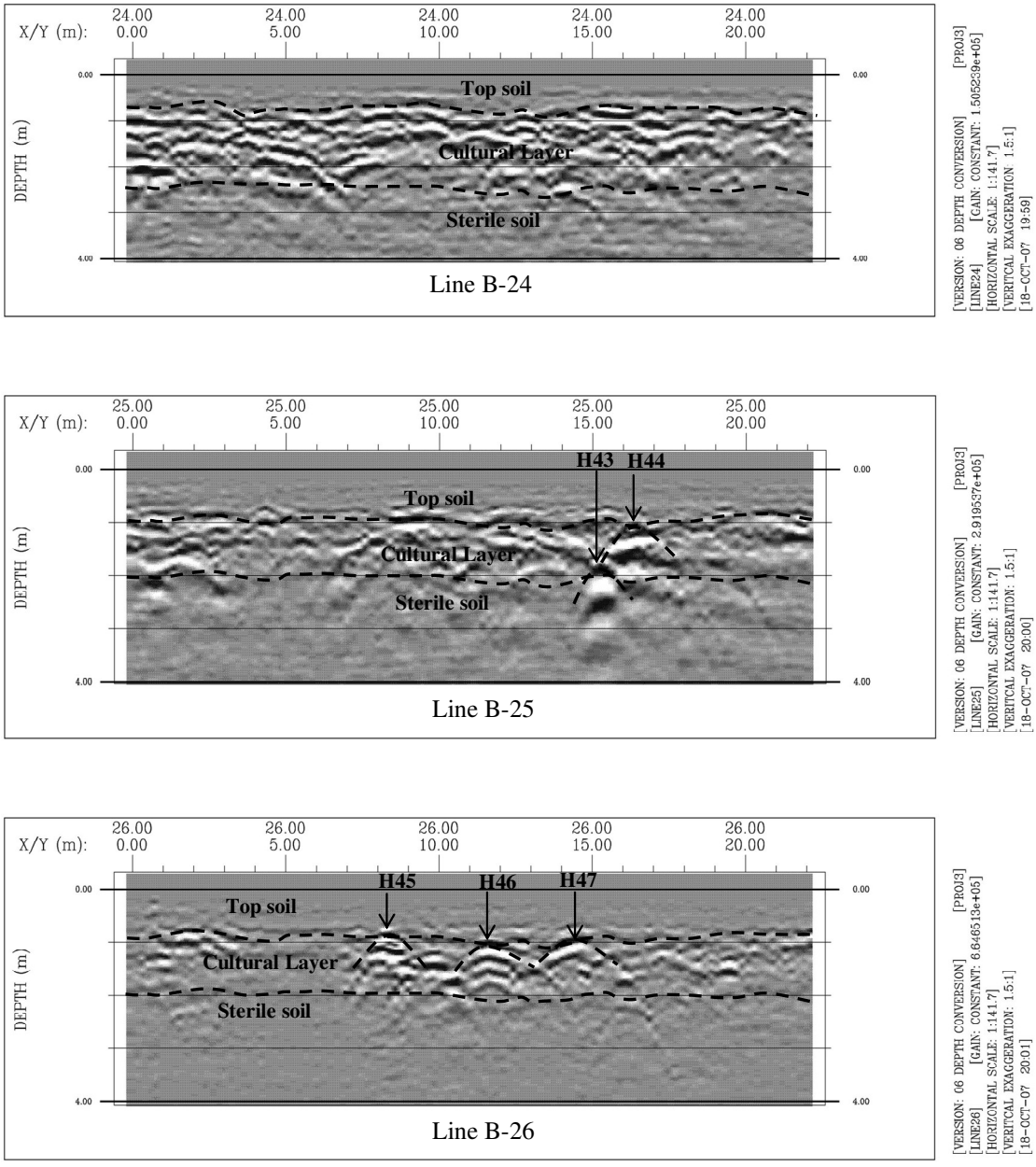

Figure 3.22 Radar section of Line B-24 to B-26

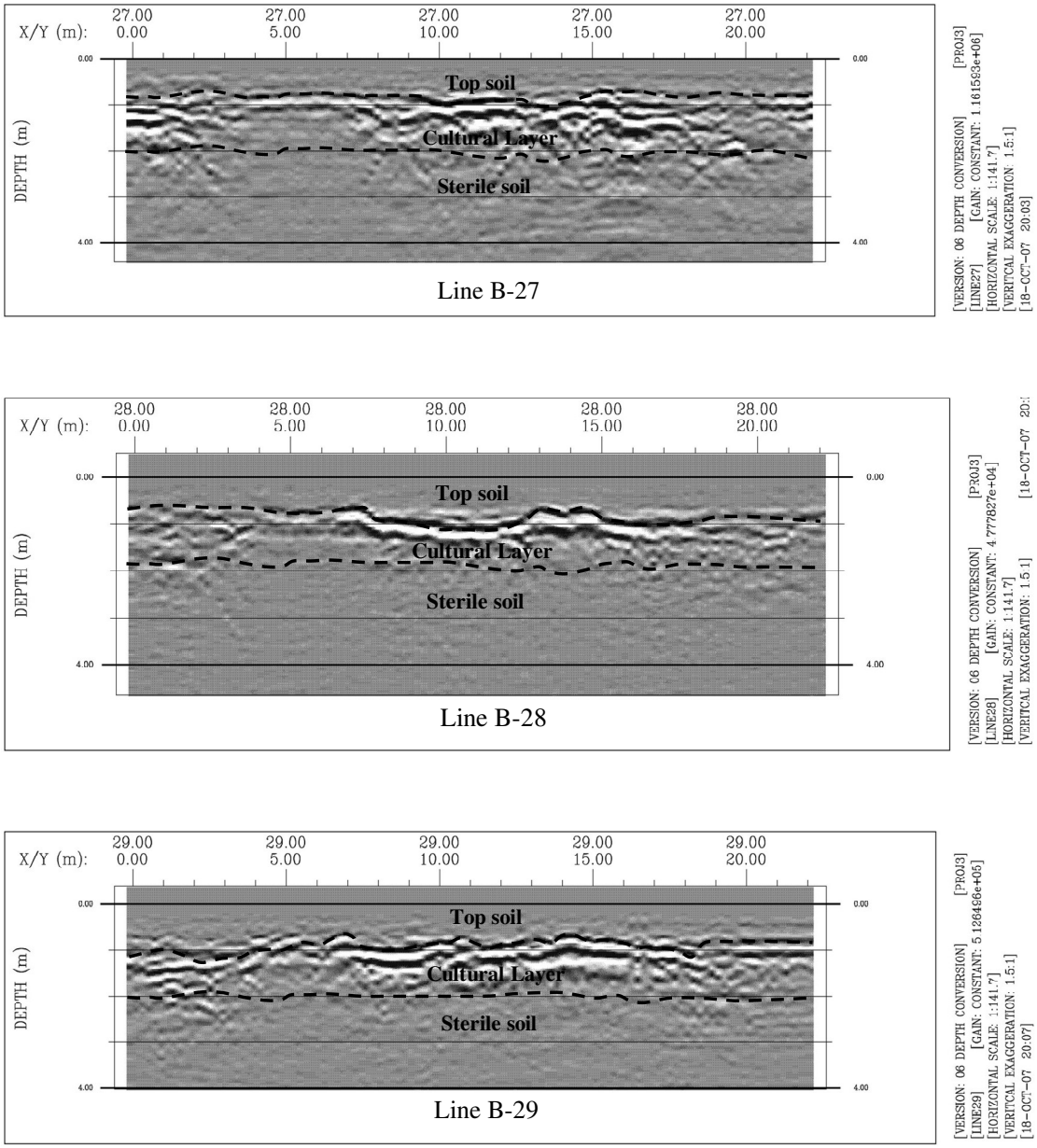

Figure3.23 Radar section of Line B-27 to B-29

3.2 Magnetic mapping

The results of the magnetic measurement in both sub-areas at two levels of sensor (height of 1.25 m and 1.85 m) are described in this section as follows;

3.2.2 Sub-areas A

The contour map of total magnetic field at height of 1.25 m above the ground is shown in Figure 3.24 (a) and moderate field of 43,629 to 43,641 nT is observed in most part of the study area. However, very high magnetic anomaly, labeled "A" of 43,755 to 43690 nT, appearing between distances 0.0 and 7.0 m on lines A-00 to A-06 is probably disturbed field from a nearby bungalow. In addition, other two anomalies, "B" and "C" are also observed in the study area. The anomaly "B" appearing between distances 2.0 and 6.0 m on lines A-12 to A-18 is probably caused by a small hut in that region, whereas anomaly "C" appearing between distances 9.0 and 11.0 m on lines A-18 to A-20 is probably caused by an iron pole in vicinity of the measuring lines.

The contour map of total magnetic field at height of 1.85 m above the ground is shown in Figure 3.24 (b) and low field of 43,620 to 43,634 nT is observed in most parts of the study area. Generally, the feature contour map at this elevation is similar to the contour map at the field at 1.25 m high.

The residual magnetic anomaly obtained from subtracting the total field of the high level sensor (1.85 m high) from the field of the low level sensor (1.25 m high) is shown in Figure 3.24 (c). The residual anomaly ranges between -22 nT and 34 nT with an average anomaly of 7 ± 3 nT. If this average residual anomaly is considered to be the background anomaly, an anomaly of which higher or lower amplitude than this background level is considered to be a significant anomaly. As a result, three residual anomalies (A, B, and C) related to man-made magnetic object on the ground are observed. Therefore, no residual magnetic anomaly related to buried-magnetic objects is observed in this sub-area.

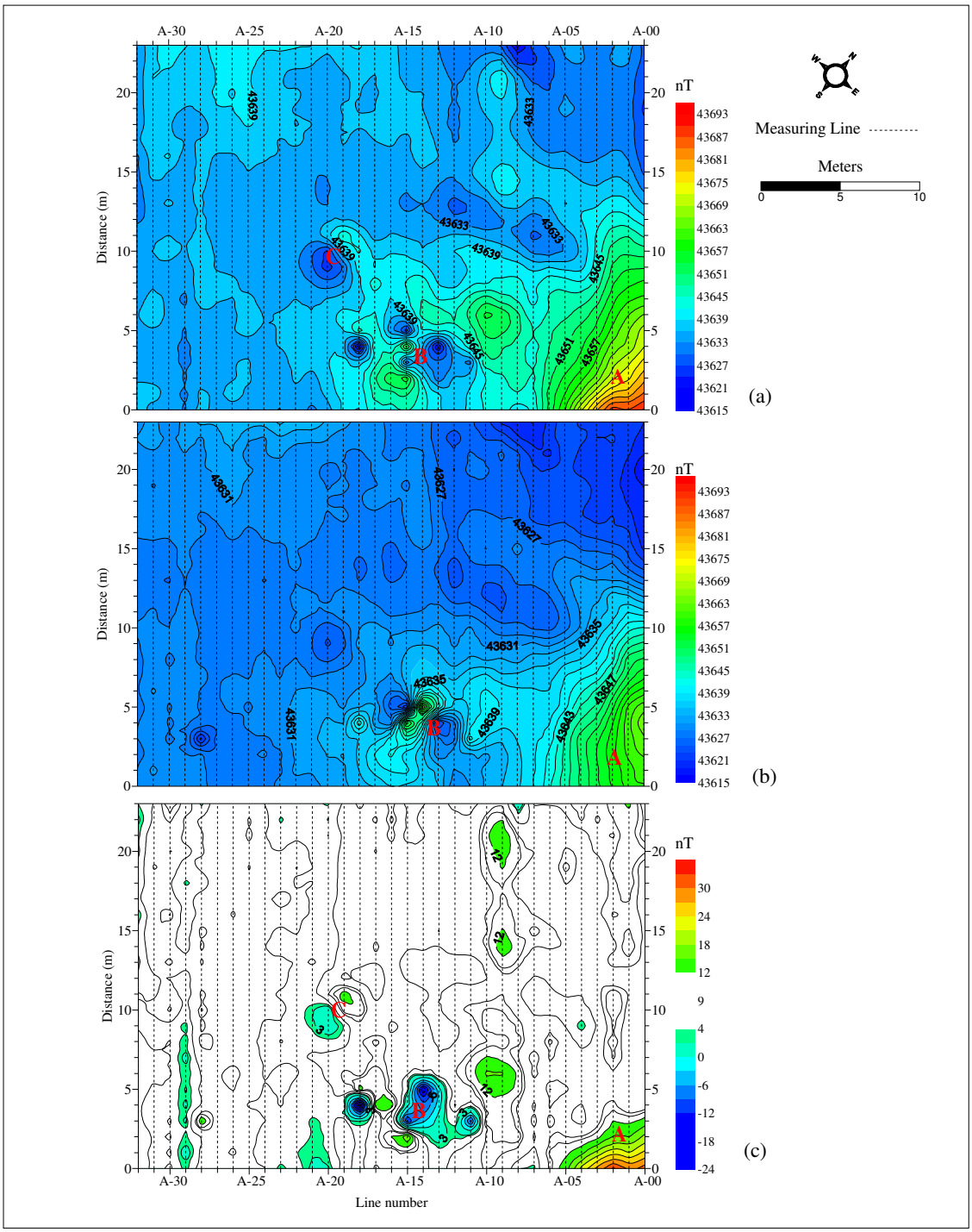

Figure 3.24 Contour map of magnetic in sub-area A; (a) and (b) contour map of total magnetic at height of 1.25 m and 1.85 m above the ground, and (c) contour map of residual magnetic field.

3.2.2 Sub-areas B

The contour map of total magnetic field at 1.25 m high above the ground is shown in Figure 3.25 (a). Moderate field of 43,624 and 43,630 nT is observed in most parts of the study area. An anomaly of alternating high and low amplitudes, labeled as "M", is observed at distances between 11.0 to 14.0 m on lines B-05 to B-08. Another small anomaly of positive amplitude is also observed at distance of 6.0 m on line B-04 is also observed in this sub-area but this anomaly is probably related with small magnetic object near the ground surface.

The contour map of total magnetic field at 1.85 m high above the ground is shown in Figure 3.25 (b). This map is very similar to the contour map at the sensor height of 1.25 m. In addition, the anomaly "M" is also observed on the magnetic map at this level of sensor but with higher amplitude.

The contour of residual magnetic anomaly obtained from subtracting the total field of the high level sensor (1.85 m high) from the field of the low level sensor 1.25 m high is shown in Figure 3.25 (c). When an average residual anomaly of 17 ± 3 nT is considered to be the background anomaly, anomaly of which higher or lower amplitude than this background level is considered to be a significant anomaly. Anomaly "M" is also observed in this residual anomaly map. It may be caused by a buried magnetic object.

According to a quantitative interpretation, the causative body of anomaly "M" on profile AA' shown in Figure 3.25 (c) is modeled as a small 3D body of rectangular shape dipping 68 degree toward the north direction at a depth of 0.2 m below the ground surface as shown in Figure 3.26. The magnetic properties of this body are 0.006 SI in magnetic susceptibility, 1.3 in remnance ratio, -13 degree remnance inclination and 131 degree remnance declination. The physical dimensions of this body are 1 m in length, 0.8 m in width and 0.4 m in thickness.

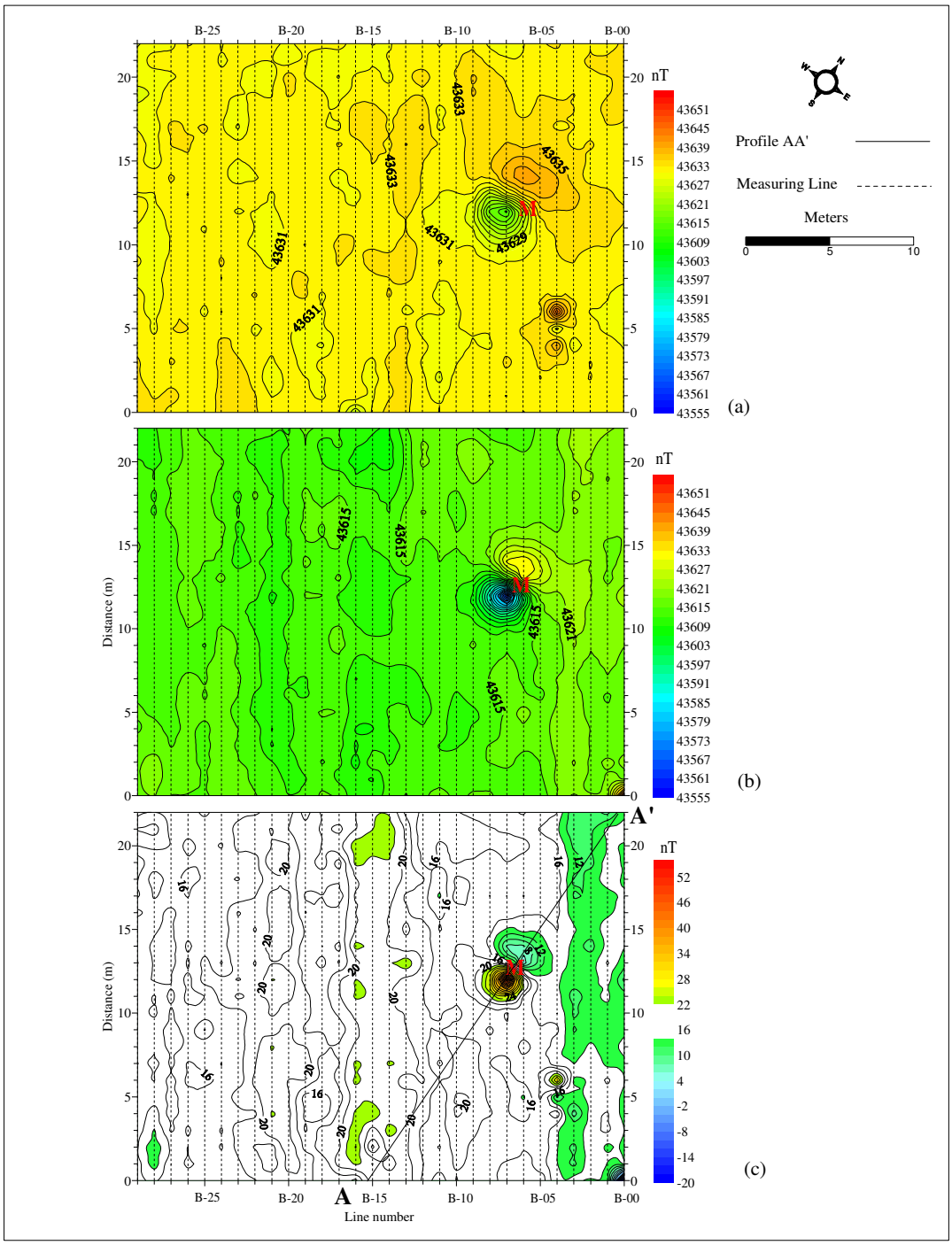

Figure 3.25 Contour map of magnetic in sub-area B; (a) and (b) contour map of total magnetic at height of 1.25 m and 1.85 m above the ground, and (c) contour map of residual magnetic field.

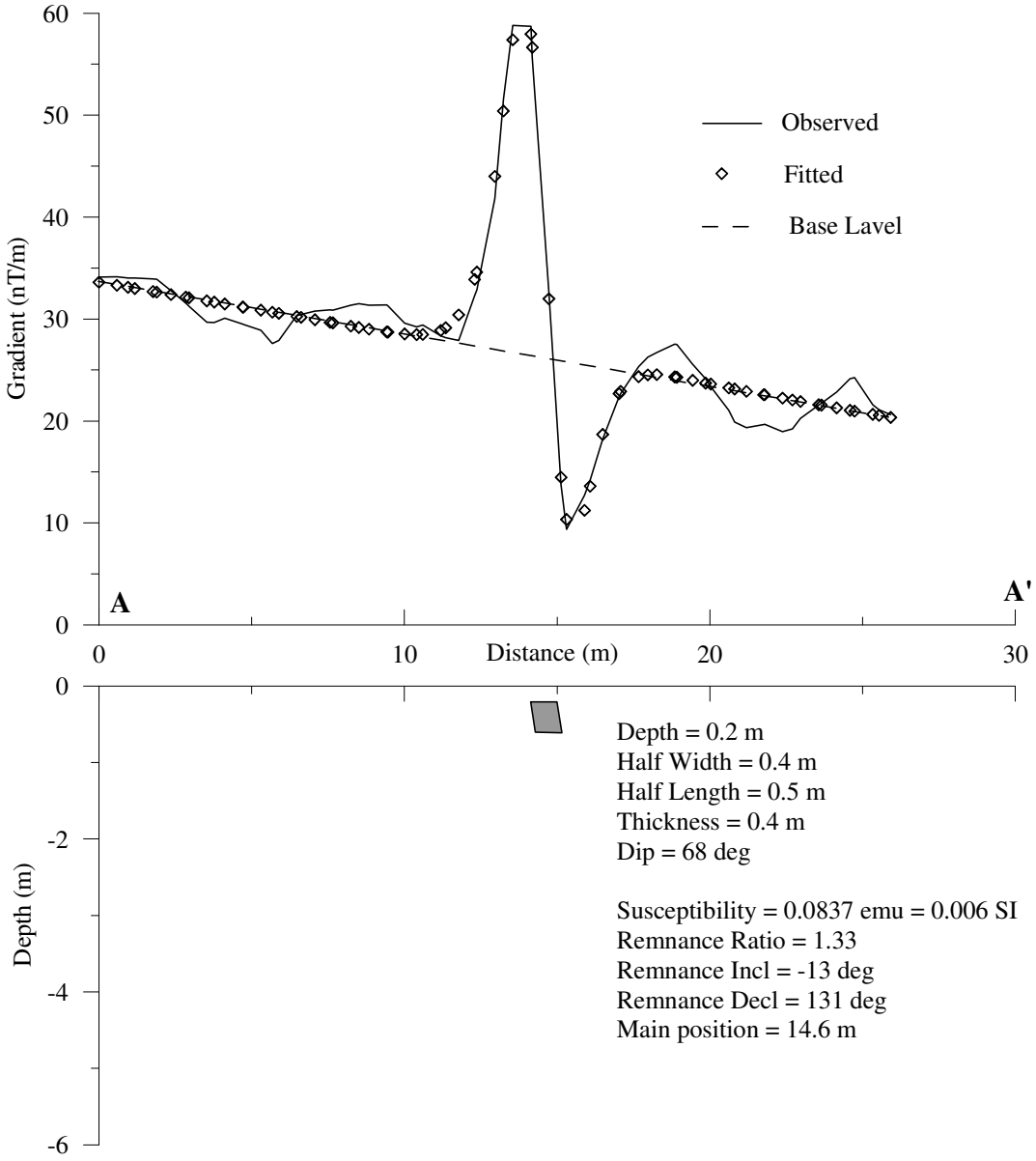

Figure 3.26 Magnetic model along the profile AA' in sub-area B.

3.3 Ground resistivity mapping

Ground resistivity mapping was conducted in the study area in order to determine zones of anomalous resistivity. Wenner configuration of electrode array with electrode spacing of 1.0 m and line spacing of 2.0 m was employed in both sub-areas, A and B, of study. According to the above electrode configuration, the effective depth of penetration is approximated to be 0.5 m (Edwards, 1977). Combined interpretation of the results obtained from resistivity mapping and GPR measurement will certainly improve our understanding on subsurface information of the study area.

3.3.1 Sub-area A

The contour map of apparent resistivity for sub-areas A is shown in Figure 3.27. An average logarithmic value of apparent resistivity of 3.32 ± 0.29 (or apparent resistivity between 4,074 to 1,072 Ωm) is observed in most parts of the study area and is considered to be a background value in this sub-area A. Refer to this background level, there are 2 types of anomalous resistivity zones, one, called “low resistivity zone”, of which apparent resistivity is lower than the background level and another one, called “high resistivity zone”, of which apparent resistivity is higher than the background level.

LR1, LR2, LR3, and LR4 are low resistivity zones and HR1, HR2, and HR3 are high resistivity zones as shown in Figure 3.27. Their locations are the followings; LR1 at distances 13.0 to 18.0 m between lines A-04 and A-09, LR2 at distances 13.0 to 16.0 m between lines A-11 and A-16, LR3 at distances 2.0 to 7.0 between lines A-18 and A-23, LR4 at distances 14.0 to 17.0 m between lines A-24 and A-27, HR1 at distances 2.0 to 8.0 m between lines A-09 and A-14, HR2 at distances 0.0 to 6.0 m between lines A-27 and A-32, and HR3 at distances 19.0 to 20.0 m between lines A-30 and A-31.

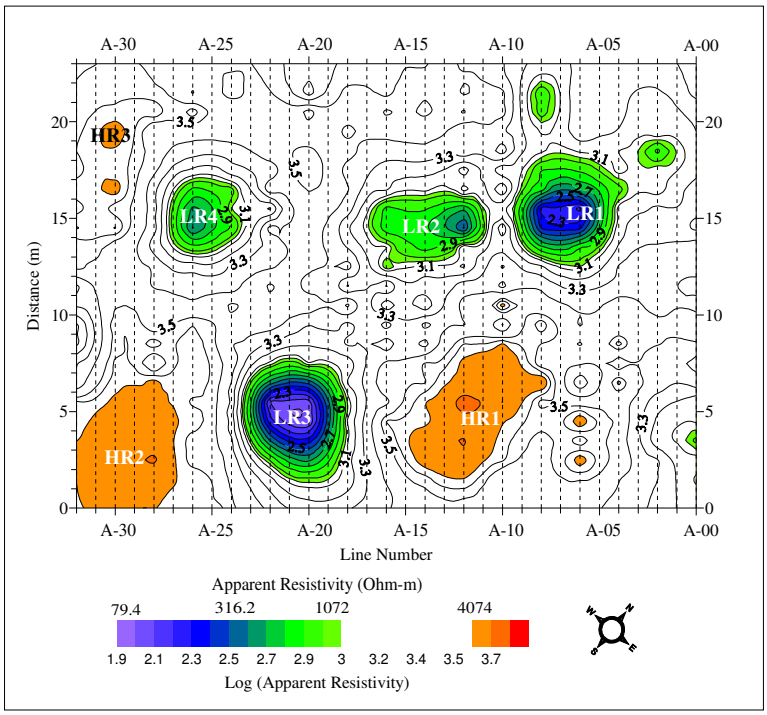

Figure 3.27 Contour map of apparent resistivity in sub-area A by using Wenner array with electrode spacing $a = 1.0$ m.

The comparison between Wenner mapping results and GPR results of sub-area A is shown in Figure 3.28. Low resistivity zones, except LR2, are observed in the same locations as the disturbed zones of radar sections. This is not true for the case if high resistivity zones. These low resistivity zones are probably areas disturbed by human activities in the past or in the present time. It should be observed that these low resistivity zones were not investigated by previous archaeological excavation pits (Källén, 2004).

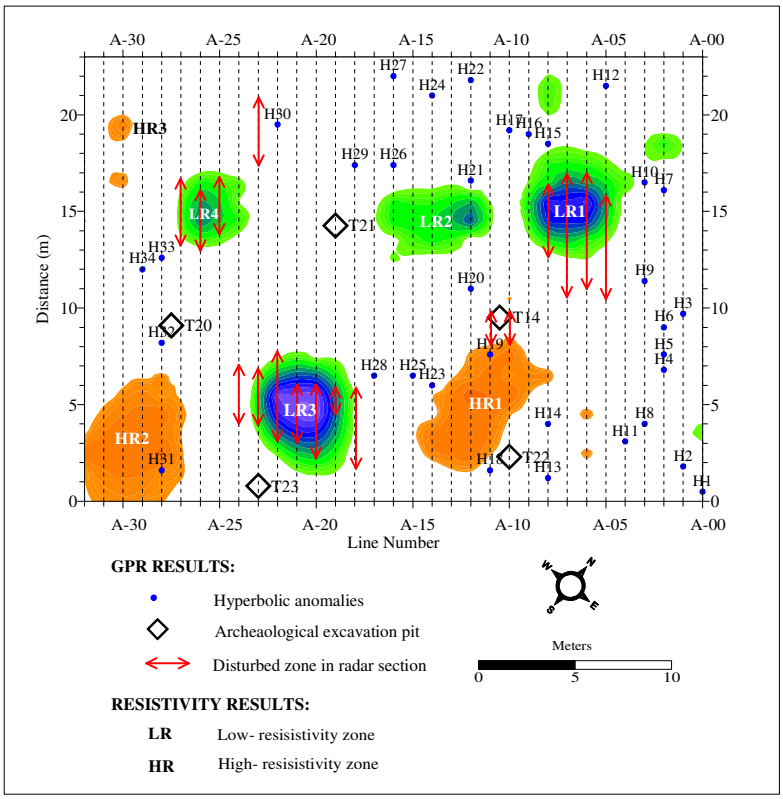

Figure 3.28 Locations of previous archeological excavation pits and anomalous zones obtained from Wenner mapping and GPR measurement in sub-areas A.

3.3.2 Sub-area B

The contour map of apparent resistivity for sub-areas B is shown in Figure 3.29. An average logarithmic value of apparent resistivity of 3.35 ± 0.28 (or apparent resistivity of 4,626 to 1,175 Ωm) is observed in most parts of the study area and is considered to be a background value in this sub-area B. Refer to this background level, there are 2 types of anomalous resistivity zones, one, called "low resistivity zone", of which apparent resistivity is lower than the background level and another one, called "high resistivity zone", of which apparent resistivity is higher than the background level.

LR5 and LR6 are low resistivity zones whereas HR4 and HR5 are high resistivity zones in sub-area B as shown in Figure 3.29. Their locations are the

followings; LR5 at distances 17.0 to 22.0 m between lines B-05 and B-25, LR6 at distances 1.0 to 10.0 m between lines B-25 and B-29, HR4 at distances 13.0 to 14.5 m between lines B-09 and B-11, and HR5 at distances 5.0 to 12.0 m between lines B-03 and B-08.

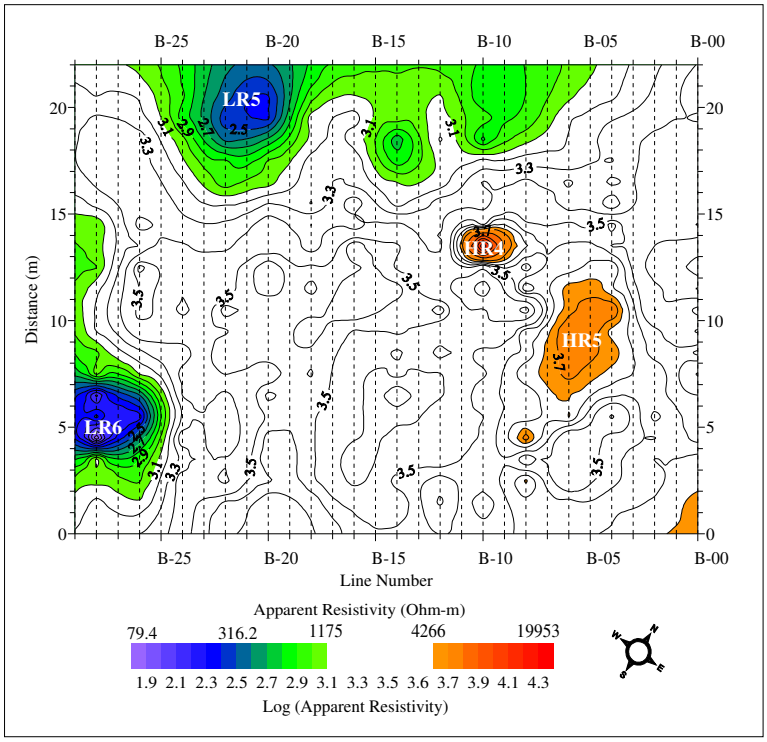

Figure 3.29 Contour map of apparent resistivity in sub-area B by using Wenner array with electrode spacing $a = 1.0$ m.

The comparison between Wenner mapping results and GPR results of sub-area A is shown in Figure 3.30. Only one low resistivity zones, LR5, are observed in the same locations as the disturbed zones of radar sections. This is not true for the case if high resistivity zones. These low resistivity zones are probably areas disturbed by human activities in the past or in the present time. It should be observed that these low resistivity zones were not investigated by previous archaeological excavation pits (Källén, 2004).

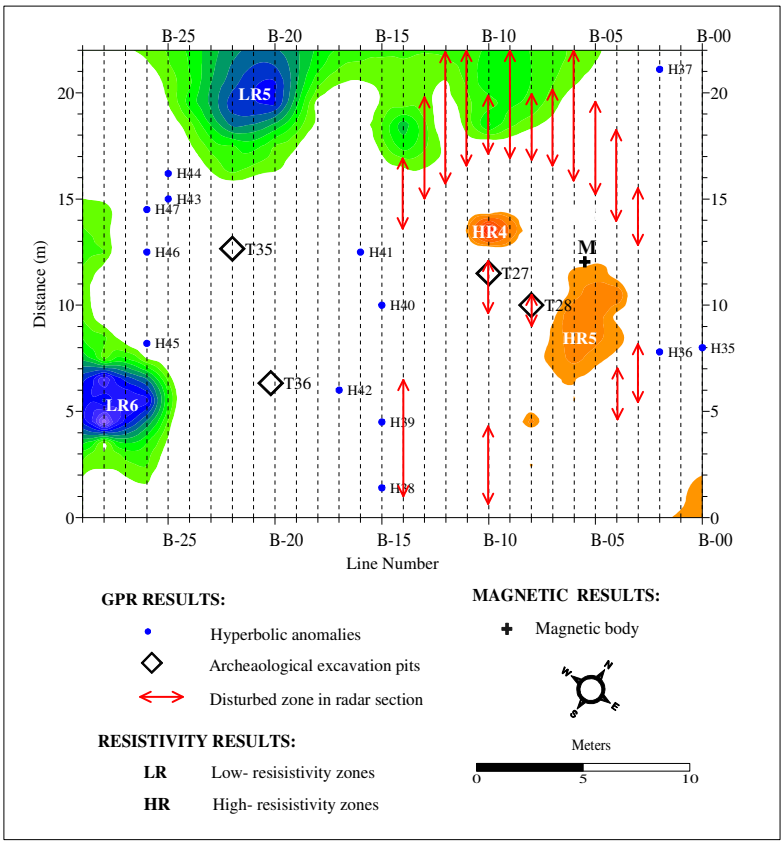

Figure 3.30 Locations of previous archeological excavation pits and anomalous zones obtained from Wenner mapping and GPR measurement in sub-area B.

3.4 CVES results

CVES measurement was carried out on some selected GPR lines of which disturbed zones in radar sections are observed. They are lines A-06, A-17, A-26, A-27 and A-28 in sub-area A and lines B-04, B-07 and B-08 in sub-area B. The purpose of this CVES measurement is to search for resistivity information of the disturbed zones in radars sections which might be related to archaeological artifacts or zones of human activity in the past.

3.4.1 Sub-area A

Line A-06:

Apparent resistivity pseudosection and inverse model resistivity section of line A-06 are shown in Figures 3.31(b) and 3.31(c) respectively. These resistivity sections are compared with Wenner mapping (Figure 3.31(a)) and radar section (Figure 3.31(d)) on the same line.

A low resistivity zone of 70 to 150 Ωm in a surrounding ground of greater than 1,000 Ωm is observed on both apparent resistivity pseudosection and inverse model resistivity section between distances 12.0 to 18.0 m. This low resistivity zone, named "L", appears at the same location as a drop to 200 Ωm in apperent resistivity obtained from Wenner mapping (Figure 3.37(a)) and the disturbed zone named "D" on radar section (Figure 3.37(d)). In addition, it can be observed that surrounding ground of which resistivity is greater than 1,000 Ωm corresponds very well with the cultural layer in the radar section. Moreover, there is a bottom layer of the inverse model of which resistivity is less than 150 Ωm. This bottom layer corresponds with sterile soil in radar section.

Line A-17:

Apparent resistivity pseudosection and inverse model resistivity section of line A-17 are shown in Figures 3.32(b) and 3.32(c) respectively. These resistivity sections are compared with Wenner mapping (Figure 3.32(a)) and radar section (Figure 3.32(d)) on the same line.

A low resistivity zone of less than 150 to 500 Ωm in a surrounding ground of greater than 1,000 Ωm is observed on both apparent resistivity pseudosection and inverse model resistivity section between distances 12.0 to 17.0 m. This low resistivity zone, named "L", appears at the same location as a drop to about 1,500 Ωm in apperent resistivity obtained from Wenner mapping (Figure 3.32(a)). However, disturbed zone is not clealy seen on the radar section (Figure 3.32(d)). In addition, it can be observed that surrounding ground of which resistivity greater than 1,000 Ωm corresponds very well

with the cultural layer in the radar section. Moreover, there is a bottom layer of the inverse model of which resistivity is less than 150 Ωm. This bottom layer corresponds with sterile soil in radar section.

Line A-26:

Apparent resistivity pseudosection and inverse model resistivity section of line A-27 are shown in Figures 3.33(b) and 3.33(c) respectively. These resistivity sections are compared with Wenner mapping (Figure 3.33(a)) and radar section (Figure 3.33(d)) on the same line.

A low resistivity zone of 150 to 513 Ωm in a surrounding ground of greater than 1,000 Ωm is observed on apparent resistivity pseudosection and inverse model resistivity section at distances between 12.0 to 17.0 m. This low resistivity zone, named "L", appears at the same location as a drop to 300 Ωm in apperent resistivity obtained from Wenner mapping (Figure 3.33(a)) and the disturbed zone named "D" on radar section (Figure 3.33(d)). In addition, it can be observed that surrounding ground of which resistivity greater than 1,000 Ωm corresponds very well with the cultural layer in the radar section. Moreover, there is a bottom layer of the inverse model of which resistivity is less than 150 Ωm. This bottom layer corresponds with sterile soil in radar section.

Line A-27:

Apparent resistivity pseudosection and inverse model resistivity section of line A-27 are shown in Figures 3.34(b) and 3.34(c) respectively. These resistivity sections are compared with Wenner mapping (Figure 3.34(a)) and radar section (Figure 3.34(d)) on the same line.

A low resistivity zone of 150 to 750 Ωm in a surrounding ground of greater than 1,000 Ωm is observed on apparent resistivity pseudosection and inverse model resistivity section between distances 11.0 to 18.0 m. This low resistivity zone,

named “L”, appears at the same location as a drop to 1,100 Ωm in apperent resistivity obtained from Wenner mapping (Figure 3.34(a)) and the disturbed zone named “D” on radar section (Figure 3.34(d)). In addition, it can be observed that surrounding ground of which resistivity greater than 1,000 Ωm corresponds very well with the cultural layer in the radar section. Moreover, there is a bottom layer of the inverse model of which resistivity is less than 150 Ωm. This bottom layer corresponds with sterile soil in radar section.

Line A-28:

Apparent resistivity pseudosection and inverse model resistivity section of line A-28 are shown in Figures 3.35(b) and 3.35(c) respectively. These resistivity sections are compared with Wenner mapping (Figure 3.35(a)) and radar section (Figure 3.35(d)) on the same line.

A low resistivity zone of 340 to 1,150 Ωm in a surrounding ground of greater than 1,000 Ωm is observed on both apparent resistivity pseudosection and inverse model resistivity section between distances 13.0 to 17.0 m. This low resitivity zone, named “L”, appears at the same location as a drop to 1,100 Ωm in apperent resistivity obtained from Wenner mapping (Figure 3.35(a)). However, disturbed zone is not clealy seen on the radar section (Figure 3.35(d)). In addition, it can be observed that surrounding ground of which resistivity greater than 1,000 Ωm corresponds very well with the cultural layer in the radar section. Moreover, it is likely that there is a bottom layer of the inverse model of which resistivity is less than 200 Ωm. This bottom layer corresponds with sterile soil in radar section.

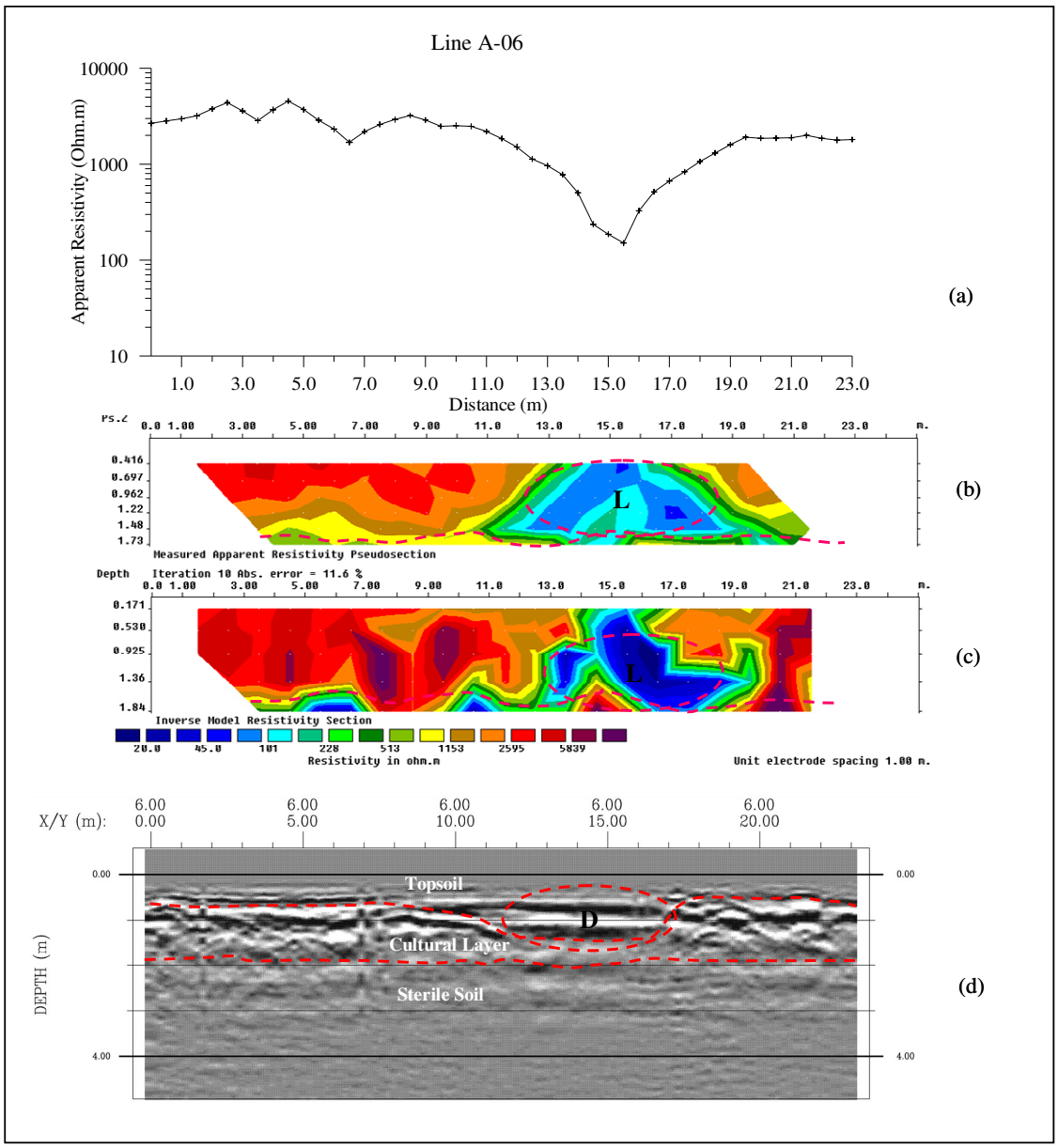

Figure 3.31 LineA-0 (a) resistivity profile using Wenner array with $a = 1.0$ m (at depth of 0.5 m), (b) measured apparent resistivity pseudosection, (c) inverse model resistivity section, and (d) radar section

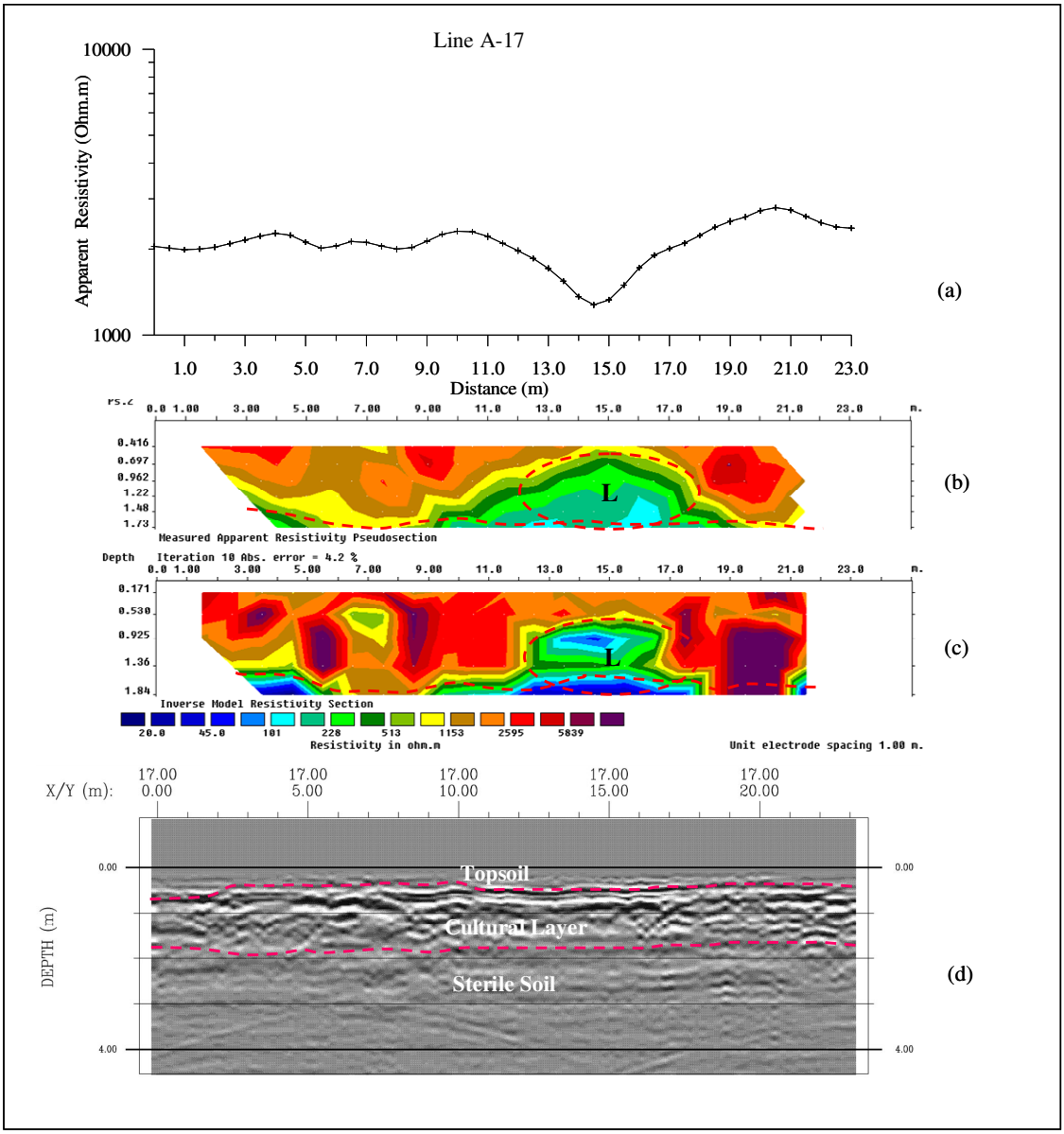

Figure 3.32 LineA-17 (a) Resistivity profile using Wenner array with $a = 1.0$ m (at depth of 0.5 m), (b) measured apparent resistivity pseudosection, (c) inverse model resistivity section, and (d) radar section

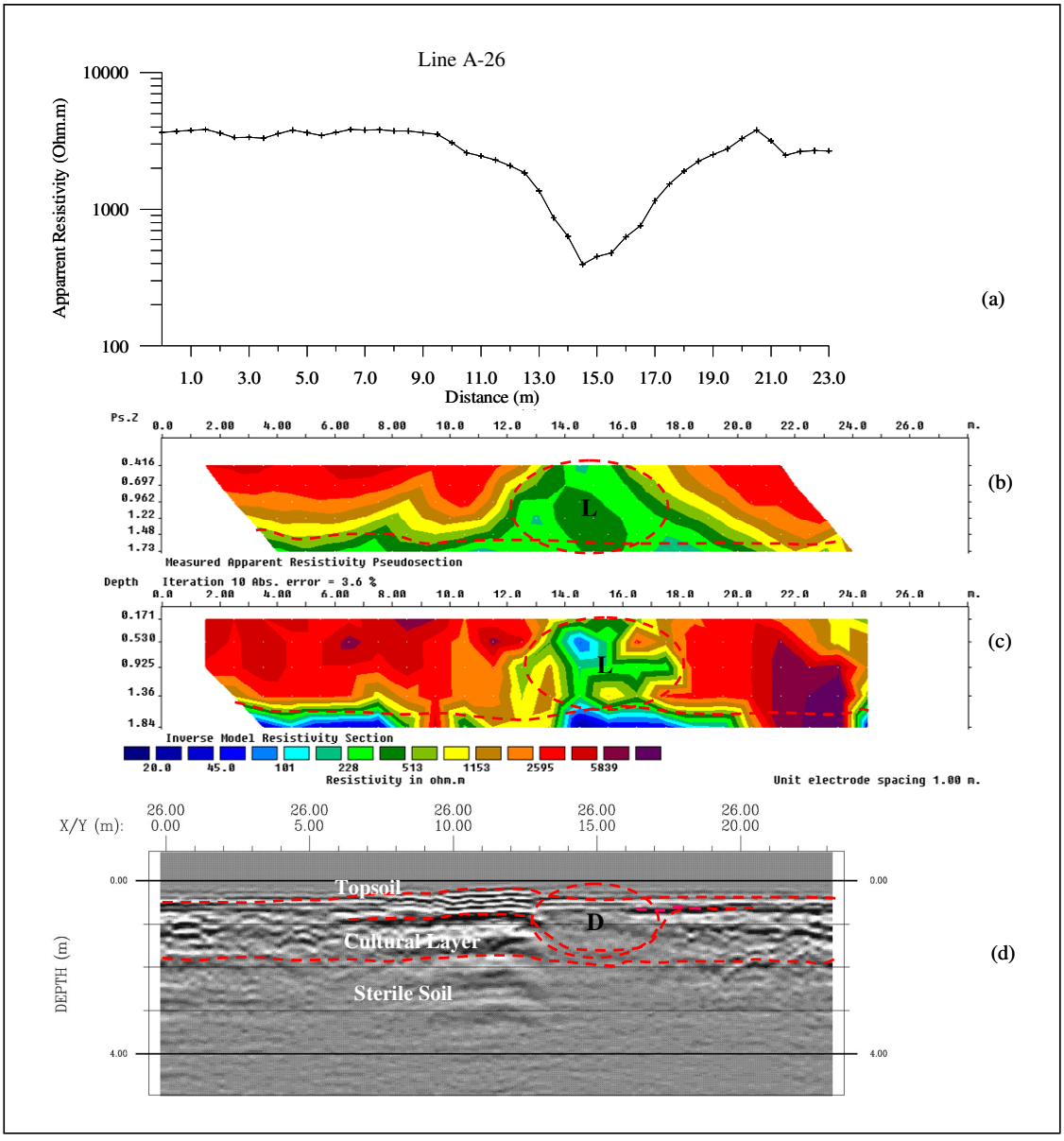

Figure 3.33 LineA-26 (a) resistivity profile using Wenner array with $a = 1.0$ m (at depth of 0.5 m), (b) measured apparent resistivity pseudosection, (c) inverse model resistivity section, and (d) radar section

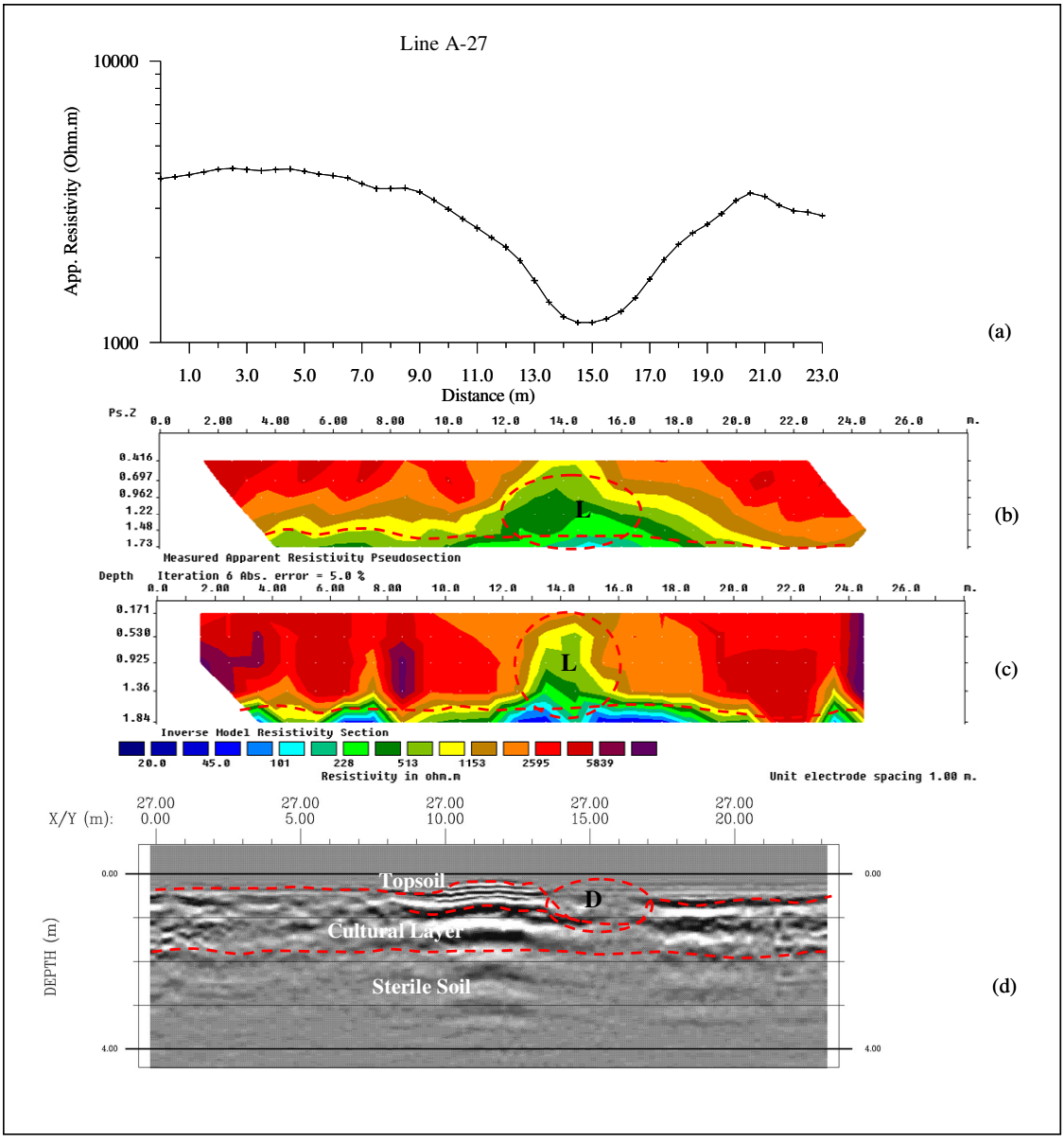

Figure 3.34 LineA-27 (a) resistivity profile using Wenner array with $a = 1.0$ m (at depth of 0.5 m), (b) measured apparent resistivity pseudosection, (c) inverse model resistivity section, and (d) radar section

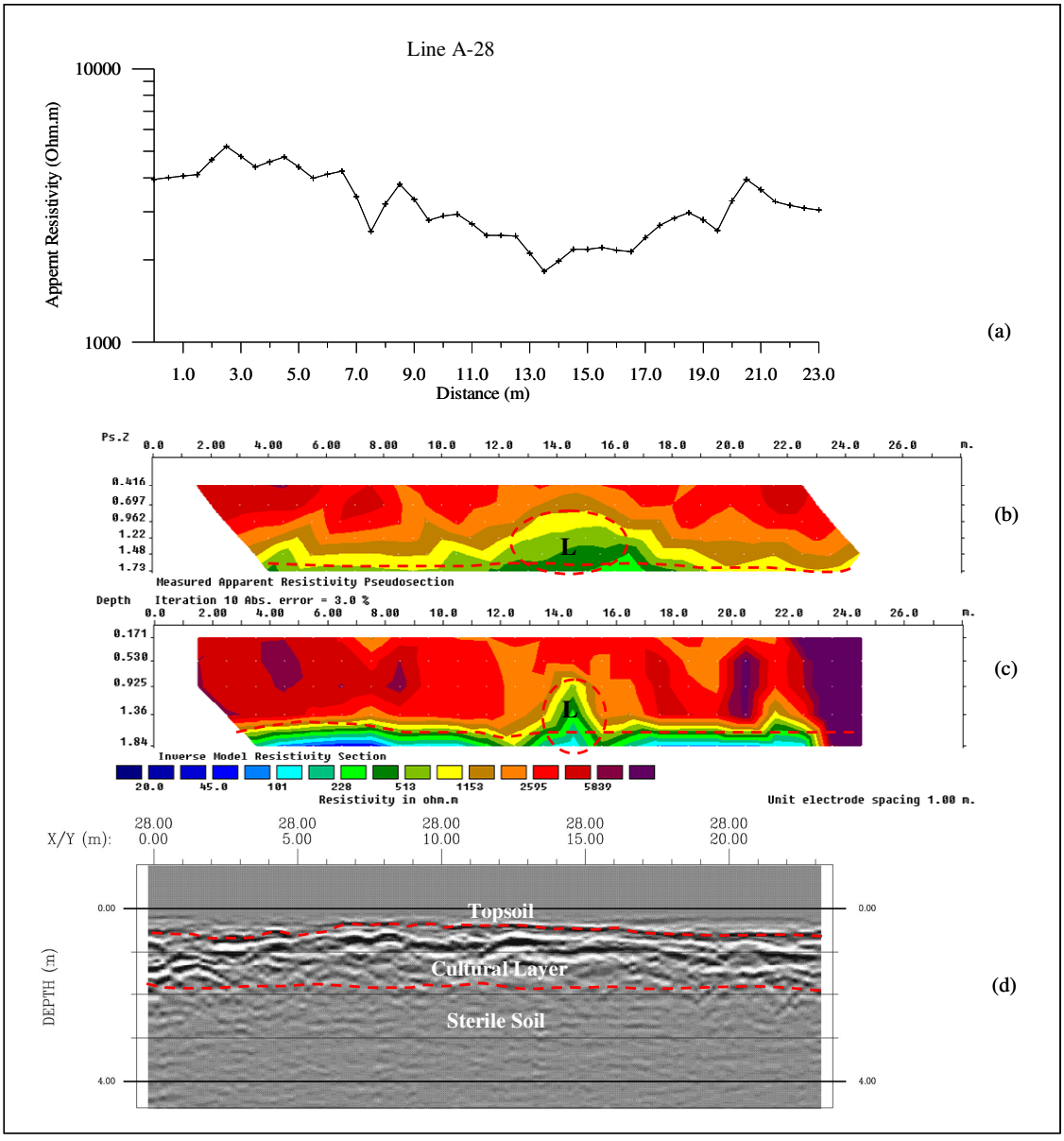

Figure 3.35 LineA-28 (a) resistivity profile using Wenner array with $a = 1.0$ m (at depth of 0.5 m), (b) measured apparent resistivity pseudosection, (c) inverse model resistivity section, and (d) radar section

3.4.2 Sub-area B

Line B-04:

Apparent resistivity pseudosection and inverse model resistivity section of line B-04 are shown in Figures 3.36(b) and 3.36(c) respectively. These resistvity sections are compared with Wenner mapping (Figure 3.36(a)) and radar section (Figure 3.36(d)) on the same line.

A low resistivity zone of 250 to 500 Ωm in a surrounding ground of greater than 1,000 Ωm m is observed on both apparent resistivity pseudosection and inverse model resistivity section between distances 17.0 to 20.0 m. This low resitivity zone, named "L", appears at the same location as a drop to 1,500 Ωm in apparent resistivity obtained from Wenner mapping (Figure 3.36(a)) and the disturbed zone named "D" on radar section (Figure 3.36(d)). This is observed at distance of 6.0-7.0 m, however, low rsisistiviy in measured apparent resistivity pseudosection and inverse model section are not clear. In addition, it can be observed that surrounding ground of which resistivity greater than 1,000 Ωm corresponds very well with the cultural layer in the radar section. Moreover, there is a bottom layer of the inverse model of which resistivity is less than 150 Ωm. This bottom layer corresponds with sterile soil in radar section.

Line B-07:

Apparent resistivity pseudosection and inverse model resistivity section of line B-07 are shown in Figures 3.37(b) and 3.37(c) respectively. These resistivity sections are compared with Wenner mapping (Figure 3.37(a)) and radar section (Figure 3.37(d)) on the same line.

A low resistivity zone of 150 to 500 Ωm in a surrounding ground of greater than 1,000 Ωm is observed on both apparent resistivity pseudosection and inverse model resistivity section at distances between 17.0 to 22.0 m. This low resistivity zone, named "L", appears at the same location as a drop to 1,000 Ωm in apparent resistivity obtained from Wenner mapping (Figure 3.37(a)) and the disturbed zone named "D" on radar section (Figure 3.37(d)). In addition, it can be observed that surrounding ground of

which resistivity greater than 1,000 Ωm corresponds very well with the cultural layer in the radar section. Moreover, there is a bottom layer of the inverse model of which resistivity is less than 150 Ωm. This bottom layer corresponds with sterile soil in radar section.

Line B-08:

Apparent resistivity pseudosection and inverse model resistivity section of line B-08 are shown in Figures 3.38(b) and 3.38(c) respectively. These resistivity sections are compared with Wenner mapping (Figure 3.37(a)) and radar section (Figure 3.37(d)) on the same line.

A low resistivity zone of 100 to 500 Ωm in a surrounding ground of greater than 1,000 Ωm is observed on both apparent resistivity pseudosection and inverse model resistivity section distances between 17.0 and 22.0 m. and 9.0 and 11.m This low resistivity zone, named "L", appears at the same location as a drop to 900 Ωm and 1,800 Ωm in apparent resistivity obtained from Wenner mapping (Figure 3.37(a)) and the disturbed zone named "D" on radar section (Figure 3.37(d)). In addition, it can be observed that surrounding ground of which resistivity greater than 1,000 Ωm corresponds very well with the cultural layer in the radar section. Moreover, there is a bottom layer of the inverse model of which resistivity is less than 150 Ωm. This bottom layer corresponds with sterile soil in radar section.

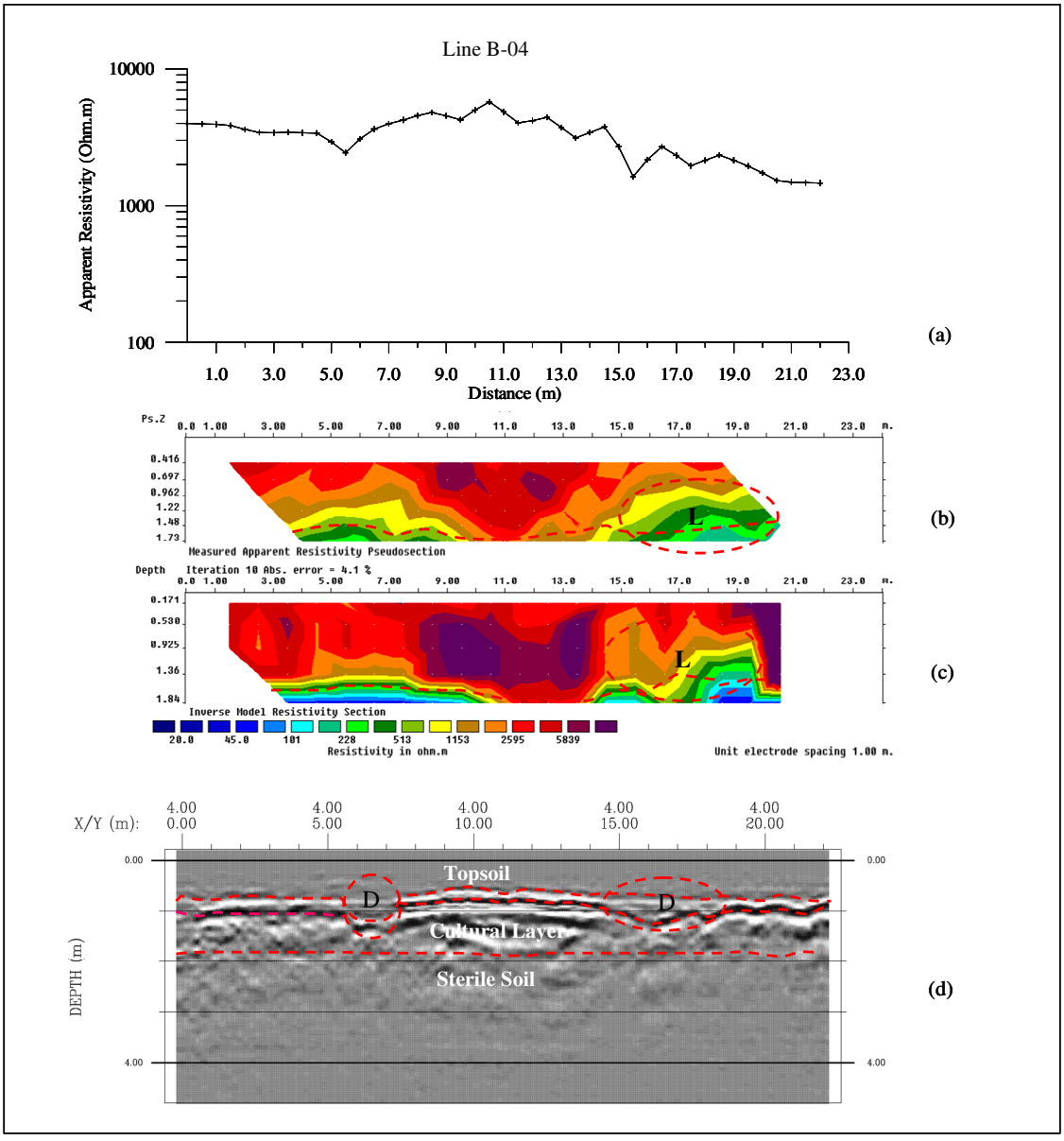

Figure 3.36 LineB-4 (a) resistivity profile using Wenner array with $a = 1.0$ m (at depth of 0.5 m), (b) measured apparent resistivity pseudosection, (c) inverse model resistivity section, and (d) radar section

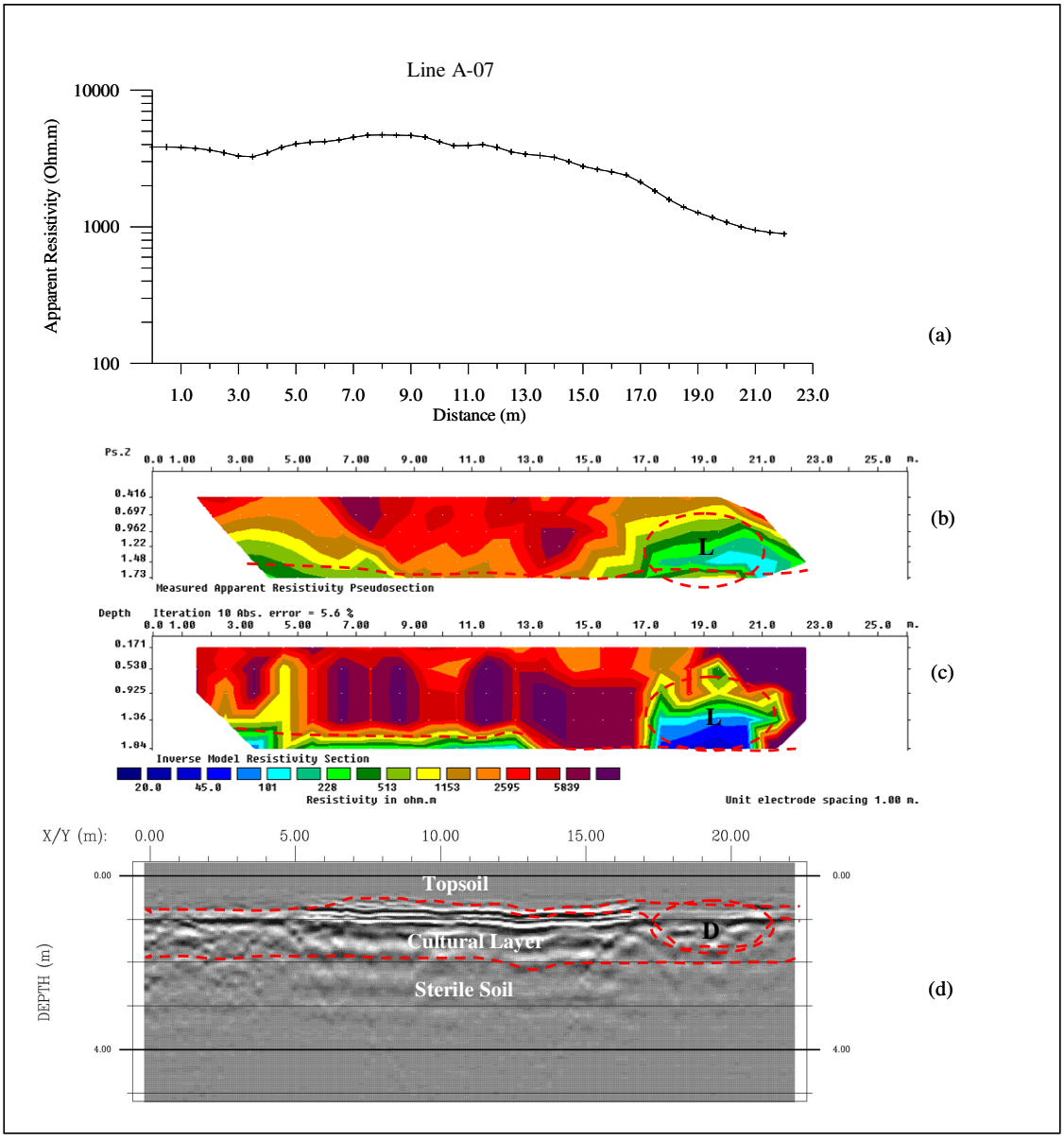

Figure 3.37 LineB-07 (a) resistivity profile using Wenner array with $a = 1.0$ m (at depth of 0.5 m), (b) measured apparent resistivity pseudosection, (c) inverse model resistivity section, and (d) radar section